Contrib Mineral Petrol (2006) 152:125–148
DOI 10.1007/s00410-006-0104-5

ORIGINAL PAPER

Experimental evidence of decompression melting during exhumation of subducted continental crust

E. Auzanneau · D. Vielzeuf · M. W. Schmidt

Received: 29 July 2005 / Accepted: 30 March 2006 / Published online: 13 June 2006

Abstract Experiments have been carried out on a metagreywacke at 800, 850 and 900°C, in the pressure range 0.5–5 GPa to locate the solidus and the eclogite/amphibolite facies transition in felsic rocks, identify the nature of the reactions responsible for major mineralogical changes, and determine the proportions of phases as a function of pressure. The mineral assemblage phengite + clinopyroxene + garnet + quartz/coesite is stable above 2.3 GPa while biotite + plagioclase + garnet + quartz is stable below 2 GPa. The model reaction for the eclogite/amphibolite facies transition in metagreywackes is:

$$\mathrm{Phe} + \mathrm{Cpx} + \mathrm{Qtz} = \mathrm{Bt} + \mathrm{Pl} + \mathrm{Grt} + \mathrm{melt}$$

with melt on the low pressure–high temperature side of the reaction. The modal proportion and calcium content of garnet change with pressure. Both decrease from 5 to 2.5 GPa, then increase at the eclogite/amphibolite facies transition, and finally decrease with decreasing pressure below 2.3 GPa. The grossular content in garnet is thus a potential marker of the eclogite/amphibolite facies transition during retrogression. The modal proportion of melt progressively increases with decreasing pressure from 5 to 2.5 GPa, then shows a sudden and marked increase between 2.5 and 2.3 GPa, and finally decreases between 2.3 and 1 GPa. Thus, a melting pulse occurs at the eclogite/amphibolite facies transition during decompression of subducted continental crust. A survey of the main UHP metamorphic regions and the P–T paths followed during their geotectonic history indicates that partial melting may have played a role during their exhumation. A striking feature of retrogressed UHP felsic rocks is that garnet rims are commonly enriched in grossular. Our experiments explain this observation and demonstrate that a grossular-rich growth zone in garnet is not necessarily indicative of highest pressures reached during metamorphism but may correspond to a decompression stage.

Communicated by F. Poitrasson

E. Auzanneau (✉)
Laboratoire Magmas et Volcans, OPGC,
CNRS et Université Blaise Pascal, 5 rue Kessler,
63038 Clermont-Ferrand, France
e-mail: estelle.auzanneau@erdw.ethz.ch

D. Vielzeuf
CRMCN-CNRS, Campus de Luminy, Case 913,
13288 Marseille cedex 9, France

M. W. Schmidt
Institute for Mineralogy and Petrology, ETH,
8092 Zurich, Switzerland

Introduction

Since the pioneering work of Verhoogen (1954, 1973), decompression of dry source materials by solid state convection in the mantle is a process invoked to generate partial melting and the production of basaltic magmas. Until recently, decompression melting has not been commonly invoked in the continental crust. There are good reasons to consider such a process not to be effective: (a) temperatures are lower than in the mantle, (b) most known melting reactions have steep dP/dT slopes, and (c) the possibility of pressure decrease is limited (Kadik and Frenkel 1980). The

characterization of ultra high pressure (UHP) coesite and/or diamond-bearing metamorphic parageneses in various orogenic belts throughout the world demonstrates that the continental crust can be brought to great depths during subduction, down to ca. 120 km (Chopin 1984; Smith 1984; Sobolev and Shatsky 1990; Coleman and Wang 1995 for a review). In such terranes, indications of partial melting are mentioned but matter of debate (Schreyer et al. 1987; Schertl et al. 1991; Sharp et al. 1993; Compagnoni and Rolfo 2000; Zhong et al. 2001; Labrousse et al. 2002; Hermann 2002; Cuthbert and Carswell 2004; Dobretsov and Shatsky 2004). On the other hand, when partial melting is identified, it remains difficult to assert whether melting predates or immediately postdates UHP metamorphism, or is a late feature in the orogenic history. Most importantly, the potential reactions responsible for the production of melt during crustal decompression, in the absence of significant ingress of H_2O, are not yet identified.

The pressure–temperature region between the wet and the dry solidi where melting may take place even in the absence of a low density fluid-phase (or in the presence of a fluid with $a_{H_2O} < 1$) is of particular importance in crustal domains. Indeed, the continental crust provides more favorable conditions than the mantle for interactions with H_2O. In most common rock types (metapelites, metagreywackes, metabasalts) several hydrous minerals may coexist with a low density fluid-phase (commonly referred to as fluid) and/or a high density fluid-phase (melt) even at relatively high temperatures and pressures (Eggler 1973; Vielzeuf and Schmidt 2001 for a review). This proliferation of hydrous phases renders partial melting phase relationships particularly complex. Considerable attention has been paid to the effect of temperature on crustal melting but only a few studies addressed the question of the influence of pressure. In the range 0.5–2 GPa, 600–900°C, two series of experiments pointed out the importance of biotite or amphibole breakdown associated with garnet forming reactions in metapelites, metagreywackes and metabasalts for the formation of melt with increasing pressure (Wyllie and Wolf 1993; Vielzeuf and Montel 1994; Vielzeuf and Schmidt 2001). However, to higher pressures (>2 GPa), only few experimental melting studies were carried out crossing the stability of biotite or amphibole with pressure (Patiño Douce and McCarthy 1998; Hermann 2002; Patiño Douce 2005).

We carried out experiments on a natural metagreywacke at three temperatures (800, 850 and 900°C) over a wide pressure range 0.5–5 GPa to (a) locate the solidus and the eclogite/amphibolite facies transition, (b) identify the nature of the reactions responsible for major mineralogical changes, (c) determine the variation of melt proportions as a function of pressure, and (d) characterize the modal and composition variations of garnet, a key mineral in these phase assemblages.

The starting material investigated in this study was used in previous studies. Vielzeuf and Montel (1994) and Montel and Vielzeuf (1997) determined the biotite fluid-absent melting relations at crustal pressures (0.1–2 GPa) and published some mineral and melt compositions up to 1 GPa. Schmidt et al. (2004) investigated the greywacke together with a MORB and a pelite at 4–7.7 GPa to determine the location of the phengite dominated solidus and the beginning of supercritical behavior. This study fills the gap in between; it focuses on the determination of the biotite to phengite transition and related melting phenomena that may occur in deeply buried continental crust.

Experimental and analytical techniques

Experimental apparatus

Internally heated pressure vessel

Gas-apparatus experiments at 0.5, 0.8 and 1 GPa were carried out in a 1.5 GPa, large volume, internally heated pressure vessel. The vessel was run horizontally, with a pressure medium of N_2, and the samples were heated by a single-zone, platinum resistance furnace. Pressure was measured by a manganin resistance cell. The variation of the pressure during an experiment was 2–5 MPa, and we estimate the pressure accuracy to be ± 10 MPa. Within the furnace, the temperature was measured by three type-B thermocouples immediately adjacent to each of the capsules and calibrated against the melting point of NaCl, $SrCl_2$, and Ag at 1 atm. The longitudinal temperature gradient was about 2°C/mm, and the variations over the duration of an experiment were comprised between 2 and 5°C.

Single stage piston cylinder

Experiments between 1 and 1.7 GPa and some at 0.5 and 0.75 GPa were carried out in a single stage, 1.91 cm, piston-cylinder apparatus. The pressure assemblies were nearly the same as those described by Vielzeuf and Clemens (1992). They comprise an outer NaCl bushing surrounding a glass sleeve, in turn surrounding the graphite furnace. Inside the furnace, an additional glass sleeve, cored by crushable magnesia, serves as the pressure medium. At the core, the small

flat Au capsule is surrounded by MgO powder. A type-C thermocouple, protected by an alumina ceramic, passes through a small hole in the magnesia. The thermocouple tip is separated from the Au capsule by a thin (< 1 mm) magnesia wafer. Independent temperature calibration experiments suggest that the difference between the temperature at the thermocouple tip and the capsule is less than 5°C. A cold pressure of 0.15 GPa was initially applied to the assembly. The temperature was then raised to approximately 510°C, at which point the pressure ceased to increase and began to decrease. Then, the desired final pressure was applied without shattering the cell. No friction correction was applied. All experiments were simultaneously brought to final P–T conditions, and we used the hot piston-in technique.

End-loaded piston cylinder

Experiments in the range 1.8–3.5 GPa were carried out in an end-loaded, 1.27 cm, piston-cylinder apparatus within a 1,000 ton press. Pressure on the sample was automatically regulated throughout the experiment. The pressure assembly is almost identical to the one used in the single stage piston cylinder; it differs by its size and the fact that the volume inside the furnace is completely filled with crushable magnesia. A factory calibrated type-C thermocouple, protected by an alumina ceramic was used. No pressure correction on EMF was applied. The sample was brought up to pressure and temperature using a protocol identical to the one for the single stage machine.

Multi-anvil

Experiments at 4 GPa and above were performed at the French CNRS-INSU multi-anvil facility, UBP-Clermont, in a Walker type multi-anvil module employing 32 mm edge length WC-cubes with 17 mm truncation edge lengths (TEL). The assembly was composed of a 25 mm edge length octahedron, a stabilized zirconia isolation sleeve, a stepped $LaCrO_3$ furnace with a graphite disc and ring between furnace and WC-cubes, and inner MgO liners. In order to avoid perforation of the capsules, an axial mullite thermocouple ceramics with approximately 30% porosity (close to the octahedron porosity of 32%) was employed together with a S-type thermocouple ($Pt\text{-}Pt_{90}Rh_{10}$). The central thickened part of the furnace contained two adjacent 1.6 mm O.D. Au capsules with their axes parallel to the furnace. Two welded Au-capsules were pressed into one cylinder (3.0 mm in diameter and 2.8 mm long) before loading in the furnace. An experiment with two thermocouples (but without capsules), placed in the predicted hot and cold spots, respectively, showed a temperature gradient less than 11°C (at 1,000°C run temperature) across the length of the capsule (Schmidt et al. 2004). Pressure was calibrated against $CaGeO_3$ garnet–perovskite (Susaki et al. 1985), and coesite–stishovite (Zhang et al. 1996) transitions at 1,000 and 800°C, respectively.

Starting materials and sample preparation

The starting material (Table 2), a natural quartz-rich metagreywacke composed of quartz (40 wt%), An_{22} plagioclase (32 wt%), and biotite (25 wt%) is described in detail by Vielzeuf and Montel (1994). It contains 1.43 wt% H_2O (determined by Karl-Fisher titration) of which 1.0 wt% is stored in biotite while the reminder may correspond to traces of chlorite in the rock and adsorbed water in the finely ground powder that cannot be driven off at 110°C. This starting material was selected for three major reasons: (1) it corresponds to a bulk composition common in the continental crust and close to the average greywacke composition of Pettijohn (1963); (2) its initial mineralogical composition is relatively simple (biotite + plagioclase + quartz); and (3) its relatively low Ca content prevents amphibole crystallization, which would result in additional H_2O-involving equilibria. A very fine rock powder (ca. 5 μm) was obtained by repeated grinding in an agate mortar under alcohol; grain size was checked under the microscope. Thin-walled Au capsules (with various sizes depending on the apparatu0s) were welded shut at one end, loaded with the starting material previously kept in a dessicator and dried at 110°C for at least 2 h before loading. Experiments lasted between 5 and 15 days. In this type of experiment, oxygen fugacity cannot be controlled by conventional buffer techniques. The presence and nature of the iron-bearing phases indicate that no drastic change in oxygen fugacity took place during the experiments.

Electron microprobe analysis, melt entrapment and mass balance procedure

Analyses were carried out on a Cameca SX100 electron microprobe at Université Blaise Pascal, Clermont-Ferrand, France. Operating conditions were 15 kV accelerating voltage and 15 nA sample current. Counting times were 10 s on peak and 5 s on the background, before and after peak measurement. Four spectrometers were used simultaneously with Na and K analyzed first to minimize losses. The following standards were used for calibration: natural albite (Si,

Na), orthoclase (K), corundum (Al), synthetic hematite (Fe), olivine (Mg), wollastonite (Ca), and $MnTiO_3$ (Mn, Ti). A ZAF correction procedure was applied. Because of the small size of the phases, backscattered electron imaging was used for phase identification. Various difficulties were encountered during the analyses:

1. *Size of the phases*: some phases are very small (less than 5 μm) and special care was required to avoid contamination by the surrounding phases. This is particularly problematic at both the lowest and highest pressures. Special difficulties arose for the following minerals: orthopyroxene (acicular shape), biotite (large but too thin), oxide minerals (very small), garnet (presence of mineral inclusions). The following criteria were approached to select the best analyses: *biotite* (normalization on the basis of 11 oxygens), no CaO, highest values of cations in the octahedral and interlayer sites; *garnet* (normalization on the basis of 12 oxygens), low or no K_2O, sum of octahedral cations close to 6; *plagioclase* (normalization on the basis of eight oxygens), no MgO and TiO_2, sum of cations close to 5, $Al \approx Na + 2Ca + K$, $Si \approx 3Na + 2Ca + 3K$, $Na + K + Ca \approx 1$; *clinopyroxene* (normalization on the basis of six oxygens, Cawthorn and Collerson 1974), low K_2O, $Si \approx 2\ X_{jd} + 2\ X_{di+hd} + 2\ X_{en+fs} + 2\ X_{Ca-esk} + X_{Ca-ts}$, $Al^{IV} \approx 2\ X_{CaTi} + X_{Cats}$; *phengite* (normalization on the basis of 11 oxygens), no CaO, sum of cations in the interlayer site close to 1, sum of cations in octahedral sites close to 2 (or slightly higher). No objective criteria could be used for the glass compositions but contamination by plagioclase was indicated by anomalously high Ca and Na contents.
2. *Loss of alkalis in glasses*: A particular problem for glass analyses concerns Na and K losses under the electron beam. Solutions commonly used to circumvent this problem, such as beam defocusing or beam displacement are difficult to apply in experiments with low melt fractions because the melt films or pools between minerals are too small. Instead of using a correction procedure as previously done (e.g. Montel and Vielzeuf 1997), we developed a new technique to obtain larger pools of melt (Vielzeuf et al. 1994). About 10 wt% coarse quartz grains (Ø ≈ 300 μm) with decrepitated fluid inclusions were mixed into the starting material. The ''porous'' quartz served as a melt trap during the experiment (Fig. 2f, f′) and analyses of melt at low fractions could be carried out with a defocused electron beam allowing minimization of alkali losses. In this configuration, quartz/coesite is the only contamination source for the melt. The compositions of contaminated glasses were corrected using the SiO_2/Al_2O_3 (wt%) ratio determined on the corresponding glass with a focused beam. A series of tests performed with 8 nA sample current showed that for our melts, minimum beam sizes of 5 and 20 μm were needed to avoid losses of K and Na, respectively. In cases where it was not possible to use such a large beam, Na concentration in the melt was determined by mass balance calculations. The addition of quartz to the starting material does not affect compositions and proportions of phases as long as the system is quartz-saturated. Other interests of the method include the facts that quartz grains are easy to polish compared to diamond aggregates and that grains from the starting material cannot penetrate into the cavities before melting.

The electron microprobe analyses of the anhydrous minerals were normalized to 100%. The best analyses were selected on the basis of the quality of the structural formulae as discussed above and used to determine an average composition of that phase in an experimental run. For the hydrous minerals, the structural formula was calculated and the chemical analyses were recalculated taking into consideration 2 OH^- per structural formula. Then the sum of the oxides (including H_2O) was normalized to 100%. The phase proportions and their standard errors were calculated through mass balance for each experiment (Table 1) using the average compositions of the phases (major elements except MnO and H_2O—all iron as FeO) and the composition of the starting material (Table 2). We used an inversion program (Albarède and Provost 1977) that incorporates analytical uncertainties in both the bulk composition and the coexisting phases. For the mineral and glass analyses, uncertainties were calculated from the statistical model of Ancey et al. (1978). For calculation, all elements have the same weight. In some cases, when the melt composition was unavailable, we carried out the mass balance calculation with the melt composition from the experiment performed at the closest P–T conditions. We used the same mass balance procedure, including the same bulk composition, for experiments with or without porous quartz grains. In our calculations, we assumed that all of the H_2O in the starting material (1.43 wt%) partitions between the melt and the hydrous minerals (biotite, phengite). Thus, melt and hydrous mineral proportions determined by mass balance were used to estimate the H_2O concentration in the

Table 1 Experimental results

Run no.		*P* (GPa)	*T* (°C)	*t* (h)		Phases present	Proportions of main phases (wt%)								
							Melt	Qtz/Cs	Pl	Bt	Opx	Grt	Phe	Cpx	Melt subst.
PC2-91-13	a, c	0.50	800	428	PC 3/4	Qtz, Pl, Bt, Grt, Glass	–	37.0 ± 0.8	36.9 ± 0.8	23.3 ± 0.8	–	2.1 ± 0.7	–	–	
A99	a, b	0.50	851	425	IH	Qtz, Pl, Opx, Glass (Mag, Ti-Mag)	55.5 ± 5.6	16.4 ± 2.3	15.4 ± 3.2	–	9.3 ± 0.4	–	–	–	
A117-A	a, b	0.50	898	350	IH	Qtz, Pl, Opx, Hc, Glass (Mag)	50.8 ± 2.5	14.6 ±2.3	21.9 ± 3.2	–	10.8 ±0.7	–	–	–	
PC1-91-19	a, c	0.75	830	412	PC 3/4	Qtz, Pl, Bt, Grt, Glass	5.9 ± 2.8	36.9 ±1.1	31.8 ± 1.8	18.7 ± 1.1	–	5.9 ±0.8	–	–	1.50–850
A109-C	a, b	0.80	855	305	IH	Qtz, Pl, Bt, Ged, Grt, Glass (Mag,Ti-Mag)	20.0 ± 6.2	30.0 ±2.4	25.5 ± 2.5	16.6 ± 3.8	–	3.5 ±2.5	–	–	(b) 0.80–875
A118-A	a, b	0.80	913	451	IH	Qtz, Pl, Bt, Opx, Grt, Glass (Mag, Ilm)	37.9 ± 8.5	22.9 ±3.8	22.0 ± 3.8	–0.9 ± 3.6	8.9 ± 4.4	7.1 ± 2.9	–	–	(b) 0.80–875
A113-C	a, b	1.00	803	403	IH	Qtz, Pl, Bt, St, Glass (Mag, Ti-Mag)	8.5 ± 3.2	33.8 ± 1.1	34.4 ± 2.7	19.0 ± 0.9	–	–	–	–	1.50–800
PC2-91-12	a, c	1.00	850	333	PC 3/4	Qtz, Pl, Bt, Grt, Glass	12.2 ± 3.1	35.5 ± 1.3	27.5 ± 1.9	15.7 ± 1.2	–	8.4 ± 1.0	–	–	1.50–850
PC2-91-11	a, c	1.25	850	238	PC 3/4	Qtz, Pl, Bt, Grt, Glass	10.0 ± 2.7	35.2 ± 1.1	29.0 ± 1.7	17.4 ± 1.1	–	7.7 ± 0.8	–	–	1.50–850
PC2-91-1	a, c	1.25	900	168	PC 3/4	Qtz, Pl, Bt, Grt, Glass	21.3 ± 2.4	31.3 ± 1.0	24.5 ± 1.7	10.4 ± 0.9	–	11.9 ± 0.8	–	–	1.50–900
PC2-2002-26	d	1.50	800	211	PC 3/4	Qtz, Pl, Bt, Grt, Glass	14.8 ± 3.3	34.4 ± 1.3	24.1 ± 1.9	19.1 ± 1.0	–	7.2 ± 0.8	–	–	
PC2-91-9	a, c	1.50	850	264	PC 3/4	Qtz, Pl, Bt, Grt, Glass	14.5 ± 2.7	33.7 ± 1.1	26.6 ± 1.7	14.5 ± 1.0	–	10.1 ± 0.8	–	–	1.50–850
PC2-91-14	a, c	1.50	850	306	PC 3/4	Qtz, Pl, Bt, Grt, Glass	14.8 ± 2.7	34.1 ± 1.1	25.5 ± 1.7	14.8 ± 1.0	–	10.2 ± 0.8	–	–	1.50–850
PC2-2002-24	d	1.50	850	430	PC 3/4	Qtz, Pl, Bt, Grt, Glass	14.8 ± 2.5	33.9 ± 1.1	25.4 ± 1.6	15.9 ± 1.0	–	9.4 ± 0.8	–	–	
PC2-2000-25	d	1.50	900	146	PC 3/4	Qtz, Pl, Bt, Grt, Glass	26.5 ± 2.3	30.0 ± 1.0	20.9 ± 1.7	8.5 ± 0.8	–	13.7 ± 0.8	–	–	1.50–900
PC2-2002-23	d	1.50	900	335	PC 3/4	Qtz, Pl, Bt, Grt, Glass	24.7 ± 2.4	30.1 ± 1.0	22.1 ± 1.7	8.7 ± 0.8	–	13.8 ± 0.8	–	–	
PC2-91-10	d	1.70	850	184	PC 3/4	Qtz, Pl, Bt, Grt, Glass	14.1 ± 4.0	34.0 ± 1.4	26.3 ± 2.5	15.1 ± 1.3	–	9.7 ± 1.0	–	–	1.80–850
PC3-2002-1	d	1.80	850	351	PC 1/2	Qtz, Pl, Bt, Grt, Glass (Rt)	31.8 ± 4.0	29.2 ± 1.4	15.6 ± 2.6	8.1 ± 1.2	–	14.6 ± 0.9	–	–	
PC3-2002-4	d	1.80	850	215	PC 1/2	Qtz, Pl, Bt, Grt, Glass (Rt)	23.3 ± 4.2	31.6 ± 1.4	20.5 ± 2.5	11.2 ± 1.5	–	12.7 ± 0.9	–	–	1.80–850
PC3-2002-5	d	1.80	900	265	PC 1/2	Qtz, Pl, Kfs, Bt, Grt, Glass (Rt)	28.9 ± 3.1	29.9 ± 1.2	19.2 ± 2.3	6.8 ± 0.8	–	14.5 ± 0.8	–	–	2.00–900
PC3-2001-13	d	1.90	800	228	PC 1/2	Qtz, Pl, Bt, Phe, Grt, Glass (Rt)	13.8 ± 6.1	34.6 ± 2.3	25.6 ± 2.6	18.0 ± 1.2	–	7.2 ± 0.8	0.1 ± 2.0	–	1.50–800
PCJRH-91-2	a, c	2.00	850	184	PC 1/2	Qtz, Pl, Bt, Grt, Glass, (Phe)	20.3 ± 3.3	33.1 ± 1.2	19.9 ± 2.1	12.7 ± 0.8	–	13.7 ± 1.0	–	–	2.30–850
PCJRH-92-5	a, c	2.00	900	192	PC 1/2	Qtz, Pl, Bt, Kfs, Grt, Glass (Rt)	36.2 ± 3.4	28.6 ± 1.2	12.7 ± 2.5	4.8 ± 1.0	–	16.8 ± 0.9	–	–	
PC3-2001-12	d	2.10	800	228	PC 1/2	Qtz, Pl, Bt, Cpx, Phe, Grt, Glass	20.3 ± 5.9	31.3 ± 2.2	22.2 ± 3.3	17.3 ± 1.7	–	9.8 ± 0.8	–0.9 ± 2.4	–0.5 ± 2.0	
PC3-2000-9B	d	2.20	900	113	PC 1/2	Qtz, Pl, Kfs, Bt, Grt, Glass (Rt)	42.2 ± 4.1	27.0 ± 1.3	7.1 ± 3.1	5.0 ± 0.8	–	18.2 ± 0.8	–	–	
PC3-2001-7	d	2.20	900	162	PC 1/2	Qtz, Pl, Kfs, Bt, Grt, Glass, (Cpx, Rt)	38.5 ± 3.8	27.8 ± 1.2	10.3 ± 2.9	5.7 ± 0.7		17.0 ± 0.8			
PC3-2000-13B	d	2.30	850	256	PC 1/2	Qtz, Pl, Bt, Grt, Phe, Cpx, Glass (Rt)	27.2 ± 5.2	30.5 ± 1.7	15.1 ± 4.0	9.9 ± 2.1	–	15.1 ± 0.7	1.5 ± 2.1	0.4 ± 2.4	
PC3-2001-1	d	2.30	850	198	PC 1/2	Qtz, Pl, Kfs, Bt, Grt, Phe, Cpx, Glass (Rt)	25.7 ± 6.2	30.0 ± 2.0	13.0 ± 5.3	4.7 ± 3.5	–	11.8 ± 0.9	6.3 ± 2.9	8.0 ± 3.1	

Table 1 continued

Run no.		*P* (GPa)	*T* (°C)	*t* (h)		Phases present	Proportions of main phases (wt%)								
							Melt	Qtz/Cs	Pl	Bt	Opx	Grt	Phe	Cpx	Melt subst.
PC3-2000-5	d	2.40	800	238	PC 1/2	Qtz, Cpx, Phe, Grt, Glass, (Bt, Rt)	5.7 ± 3.2	37.3 ± 1.3	–	–	–	7.2 ± 0.8	24.2 ± 1.6	25.0 ± 1.5	2.40–870
PC3-2000-8	d	2.40	850	162	PC 1/2	Qtz, Cpx, Phe, Grt, Glass, (Bt, Rt)	8.1 ± 3.6	34.4 ± 1.4	–	–	–	5.5 ± 1.0	20.9 ± 1.7	30.6 ± 2.0	2.40–870
PC3-2001-16	d	2.40	850	181	PC 1/2	Qtz, Cpx, Phe, Grt, Glass, (Bt, Rt)	11.2 ± 3.4	34.9 ± 1.3	–	–	–	9.6 ± 0.8	20.5 ± 1.6	23.4 ± 1.6	2.40–870
PC3-2001-11	d	2.40	870	164	PC 1/2	Qtz, Cpx, Phe, Grt, Glass (Rt)	27.0 ± 2.6	31.2 ± 1.2	–	–	–	13.6 ± 0.7	12.3 ± 1.3	15.7 ± 1.3	
PC3-2000-10	d	2.40	900	140	PC 1/2	Qtz, Cpx, Phe, Grt, Glass (Rt)	34.3 ± 2.6	27.0 ± 1.2	–	–	–	11.3 ± 1.0	9.4 ± 1.4	17.8 ± 1.7	2.40–870
PC3-2000-7	d	2.80	800	159	PC 1/2	Qtz, Cpx, Phe, Grt (Rt)	–	38.8 ± 0.7	–	–	–	7.9 ± 0.6	25.6 ± 0.7	26.9 ± 0.9	
PC3-2000-12	d	2.80	900	136	PC 1/2	Qtz, Cpx, Phe, Grt, Glass (Rt)	25.5 ± 3.0	31.7 ± 1.3	–	–	–	11.8 ± 0.9	12.7 ± 1.4	17.7 ± 1.6	2.40–870
PC3-2001-10	d	3.30	900	169	PC 1/2	Cs, Cpx, Phe, Grt, Glass (Rt)	11.9 ± 3.9	36.3 ± 1.5	–	–	–	10.0 ± 0.9	17.3 ± 1.6	23.8 ± 1.9	2.40–870
ME36	e	4.00	790	141	ME	Cs, Cpx, Phe, Grt (Rt)	–	39.3 ± 0.9	–	–	–	11.9 ± 0.7	21.3 ± 0.7	26.5 ± 0.9	
ME35	e	4.00	850	96	ME	Cs, Cpx, Phe, Grt (Rt)	–	38.9 ± 1.3	–	–	–	11.7 ± 1.0	21.3 ± 1.1	27.1 ± 1.5	
ME32	e	4.00	900	60	ME	Cs, Cpx, Phe, Grt, Glass (Rt)	20.7 ± 3.9	30.9 ± 1.8	–	–	–	14.9 ± 0.8	10.0 ± 2.3	23.5 ± 0.9	
ME207	e	5.00	850	143	ME	Cs, Cpx, Phe, Grt (Rt)	–	39.8 ± 1.0	–	–	–	12.0 ± 0.7	21.7 ± 0.8	25.4 ± 1.0	
ME142	e	5.00	900	162	ME	Cs, Cpx, Phe, Grt, Glass (Rt)	10.3 ± 2.9	36.1 ± 1.3	–	–	–	13.7 ± 1.3	15.0 ± 1.8	24.2 ± 0.8	5.00–900
ME202	e	5.00	900	59	ME	Cs, Cpx, Phe, Grt, Glass (Rt)	9.0 ± 4.6	36.2 ± 2.4	–	–	–	12.9 ± 0.7	15.9 ± 3.0	25.2 ± 1.4	

Phases present in all run products: monazite, apatite, Fe-sulphides, zircon, scheelite. Origin of data: *a*: phase determinations from Vielzeuf and Montel (1994). *b*: phase analysis from Montel and Vielzeuf (1997). *c*: phase analysis from the present study. *d*: phase determinations and analysis from this study. *e*: phase determinations and analysis from Schmidt et al. (2004). *Melt subst.* in the absence of available melt composition, the mass balance calculation was carried out using the melt composition from another experiment at the closest *P–T* conditions (GPa–°C)

Abbreviations: *IH* internally heated gas apparatus, *PC* piston cylinder, *ME*, multi-anvil, *t* duration of the experiment measured from the attainment of the desired temperature to the quench. *Bt* biotite, *Cpx* clinopyroxene, *Cs* coesite, *Ged* gedrite, *Grt* garnet, *Hc* hercynite, *Ilm* ilmenite, *Kfs* alkali feldspar, *Mag* magnetite, *Opx* orthopyroxene, *Phe* phengite, *Pl* plagioclase, *Qtz* quartz, *Rt* rutile, *St* staurolite, *Ti-Mag* titano-magnetite

Table 2 Composition of the starting material CEVP and representative compositions of minerals and melts normalized to 100% in the range 2.1–2.4 GPa, 800–900°C

Ref.	*P* (GPa)	*T* (°C)		SiO_2	TiO_2	Al_2O_3	FeO	MnO	MgO	CaO	Na_2O	K_2O	H_2O	Total
CEVP				69.99	0.70	12.96	4.82	0.06	2.36	1.67	2.95	2.41	1.43	99.35
PC3-2001-12	2.1	800	Grt	38.49	0.52	21.29	26.87	0.55	5.35	6.81	0.12	0.01		100.00
			Bt	42.12	3.79	17.65	11.80	0.00	10.51	0.06	0.66	9.23		95.82
			Pl	62.96	0.03	22.96	0.26	0.01	0.06	4.23	8.84	0.65		100.00
			Phe	50.74	1.28	27.12	2.85	0.00	3.17	0.02	0.96	9.20		95.32
			Cpx	55.72	0.42	13.26	5.47	0.03	6.82	11.30	6.83	0.15		100.00
PC3-2000-9B	2.2	900	Grt	38.04	1.17	21.58	23.61	0.64	8.46	6.25	0.19	0.07		100.00
			Bt	41.46	4.92	18.70	6.11	0.00	14.43	0.05	0.51	9.54		95.73
			Pl	64.09	0.03	21.90	0.24	0.01	0.02	3.31	8.69	1.71		100.00
			Kfs	66.02	0.00	19.10	0.24	0.00	0.00	0.49	5.70	8.46		100.00
			Melt	70.35	0.26	15.56	0.51	0.04	0.23	0.77	5.39[a]	4.28	2.88[a]	100.27
PC3-2001-7	2.2	900	Grt	37.97	1.08	21.55	24.83	0.48	8.03	5.81	0.21	0.04		100.00
			Bt	40.48	4.97	17.80	6.75	0.00	15.70	0.04	0.58	9.45		95.76
			Pl	63.97	0.05	21.82	0.23	0.01	0.03	3.29	8.79	1.81		100.00
			Kfs	65.91	0.05	19.27	0.20	0.00	0.00	0.70	6.37	7.50		100.00
			Melt	70.03	0.19	15.68	0.52	0.00	0.25	0.96	5.12[a]	4.37	3.09[a]	100.21
PC3-2000-13B	2.3	850	Grt	38.00	0.88	21.42	25.72	0.80	5.96	7.02	0.15	0.07		100.00
			Bt	42.26	4.26	18.51	7.50	0.01	13.02	0.06	0.75	9.38		95.74
			Pl[b]	64.43	0.05	21.96	0.32	0.03	0.12	2.81	9.30	0.98		100.00
			Phe[b]	49.55	2.96	26.36	1.85	0.00	3.90	0.08	1.24	9.45		95.39
			Melt	69.83	0.21	15.09	0.57	0.03	0.26	0.48	5.19	4.34	3.46[a]	99.46
PC3-2001-1	2.3	850	Grt	38.11	1.00	21.56	27.49	0.74	7.47	3.42	0.16	0.06		100.00
			Bt[b]	40.27	4.33	20.26	10.57	0.04	10.33	0.18	0.89	8.93		95.80
			Pl	63.92	0.31	21.49	0.82	0.00	0.59	3.03	8.01	1.83		100.00
			Kfs	65.52	0.03	19.19	0.28	0.04	0.01	0.51	4.61	9.82		100.00
			Phe	50.89	1.98	25.52	2.89	0.00	3.46	0.10	0.58	9.92		95.34
			Cpx	54.52	0.39	14.58	7.42	0.21	7.10	9.63	5.91	0.24		100.00
PC3-2000-5	2.4	800	Grt	37.71	0.82	21.20	30.68	0.41	4.64	4.27	0.22	0.05		100.00
			Phe	49.91	1.66	26.00	4.06	0.00	3.90	0.06	1.06	8.63		95.28
			Cpx	56.40	0.57	17.32	6.09	0.19	4.16	5.75	9.39	0.11		100.00
PC3-2000-8	2.4	850	Grt	38.80	0.62	21.26	29.84	0.30	5.91	2.98	0.24	0.06		100.00
			Phe	49.87	1.81	26.84	3.41	0.01	3.06	0.06	0.96	9.29		95.31
			Cpx	57.22	0.50	17.26	7.35	0.19	3.98	4.65	8.81	0.05		100.00
PC3-2001-16	2.4	850	Grt	38.47	1.03	20.90	28.90	0.47	6.11	3.75	0.33	0.04		100.00
			Phe	49.65	2.32	25.89	3.03	0.01	3.80	0.08	0.88	9.69		95.35
			Cpx[b]	57.01	0.50	16.93	6.69	0.13	4.28	5.41	8.89	0.17		100.00
PC3-2001-11	2.4	870	Grt	37.54	0.85	21.44	27.24	0.35	6.74	4.89	0.26	0.06		100.00
			Phe	49.58	2.52	26.29	2.43	0.00	3.89	0.22	0.71	9.73		95.37
			Cpx	55.53	0.59	17.19	6.22	0.14	5.41	6.38	8.46	0.09		100.00
			Melt[b]	70.30	0.17	15.09	0.48	0.06	0.20	0.28	4.98	4.43	3.06[a]	99.05
PC3-2000-10	2.4	900	Grt	38.39	0.82	21.45	27.07	0.35	7.40	4.15	0.31	0.06		100.00
			Phe	49.26	2.84	25.91	3.06	0.02	3.51	0.03	0.61	10.11		95.36
			Cpx	55.15	0.55	17.33	7.40	0.25	5.23	6.34	7.63	0.13		100.00

[a]Estimated by mass balance calculations

[b]Compositions used for balancing reaction 3

melt. In the same way, Na_2O contents in the melt were estimated considering that all of the Na_2O partitions between the melt and the sodic minerals (plagioclase, clinopyroxene).

Experimental results

Results of 22 new experiments are reported in Table 1 together with mass balancing of 14 experiments by Vielzeuf and Montel (1994), and 6 experiments from Schmidt et al. (2004). They correspond to three isothermal sections at 800, 850 and 900°C, in the pressure range 0.5–5 GPa. A selection of BSE images of the run products are shown in Fig. 2. In this paper, we will focus on four aspects related to decompression melting: (1) the variation of mineral assemblages, (2) the modal proportion of glass and garnet, (3) the variation of garnet composition, and (4) the implications

for exhuming subducted continental crust. Data will be discussed as a function of decreasing pressure.

Phases assemblages as a function of pressure

The main minerals observed in the experiments are phengite, clinopyroxene, biotite, plagioclase, quartz, coesite, garnet, and melt, plus subordinate amounts of orthopyroxene, and rare occurrences of staurolite and gedrite. Minor phases include monazite, zircon, apatite, pyrite, scheelite, spinel, ilmenite, and rutile. Crystals are most commonly euhedral, homogeneously distributed within the charge and vary in size from 3 to 15 μm (Fig. 2). Such features indicate that both chemical and textural equilibrium were reached, probably through dissolution–recrystallization processes. The phase assemblage obtained in each experiment is indicated in Table 1 and Figs. 1, 2, 3 and 4.

High pressure phases (above ca. 2 GPa)[1] Clinopyroxene and phengite are the two characteristic high pressure minerals. *Clinopyroxene* is stable down to about 2.0 GPa at 800°C, 2.1 GPa at 850°C, and 2.3 GPa at 900°C. The experimental data suggest a slightly positive slope for this boundary. With decreasing pressure, *phengite* disappears between 1.9 and 1.5 GPa at 800°C (most likely closer to 1.9 than 1.5, on the basis of modal proportions), between 2.0 and 1.8 GPa at 850°C, and between 2.4 and 2.2 GPa at 900°C. Here again, the data are consistent with a slightly positive slope for the phengite-out curve.

Low pressure phases (up to ca. 2 GPa) Drastic changes of mineralogical assemblages happen in the pressure range 2.5–1.9 GPa. *Biotite* is present in all low pressure, low temperature experiments. It appears with decreasing pressure between 2.8 and 2.4 GPa at 800°C, at about 2.4 GPa at 850°C (on the basis of its low modal proportion), and between 2.4 and 2.2 GPa at 900°C (see Fig. 1). These data suggest a slightly negative dP/dT slope for the biotite-in line. *Plagioclase* is also present in all runs at low pressure. The plagioclase-in curve is tightly constrained at high pressure: it is located between 2.4 and 2.1 GPa at 800°C, 2.4 and 2.3 GPa at 850°C, and between 2.4 and 2.2 GPa at 900°C (see Fig. 1). Note that the plagioclase-in and biotite-in curves nearly coincide, though three runs have biotite and no plagioclase. *Orthopyroxene* is observed only at low pressure (≤ 0.8 GPa) and high temperature (Table 1; Fig. 1), and is not of importance for the eclogite to amphibolite facies transition in this greywacke composition.

[1] In this paper, 'low/high' temperature or pressure terminology is relative to the experimentally studied P–T range. LT: < ca. 850°C; LP: < ca. 2 GPa.

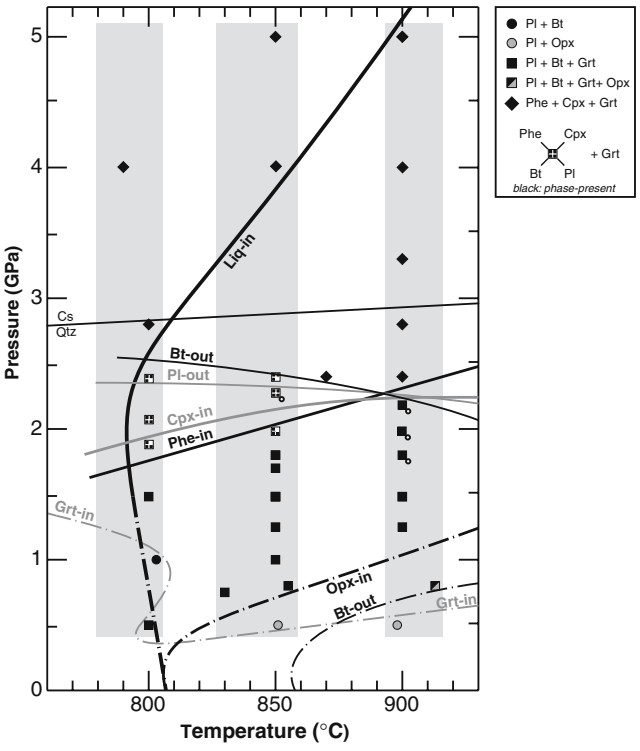

Fig. 1 Location of the main phase boundaries in pressure–temperature space. *Dash-dotted lines* after Vielzeuf and Montel (1994); Cs = Qtz from Hemingway et al. (1998). At high pressure ($P > 2.0$ GPa), the characteristic phases are phengite and clinopyroxene whereas at low pressure ($P < 2.0$ GPa), biotite and plagioclase become stable. Garnet and melt are present at both high and low pressures. For abbreviations see Table 1

Phases present at high and low pressures Garnet and melt are two phases of major interest, present at both high and low pressures; their modal proportions change drastically with pressure.

Melt and garnet proportions as a function of pressure

The variation of the modal proportion of *melt* as a function of pressure is shown in Fig. 3a–c for the three isothermal sections. From high to low pressures, four domains (I–IV) can be identified. A first melting stage (domain I) can be identified in the 900°C section (Fig. 3c) where a progressive increase in melt proportion occurs from 5.0 to 2.5 GPa. This stage is missing in the 800°C section but likely to be present in the 850°C section though not clearly characterized due to the absence of intermediate data. One of the most striking features in Fig. 3a–c is the marked increase (ca. 10–20%) in melt proportion at about 2.3 GPa (domain II),

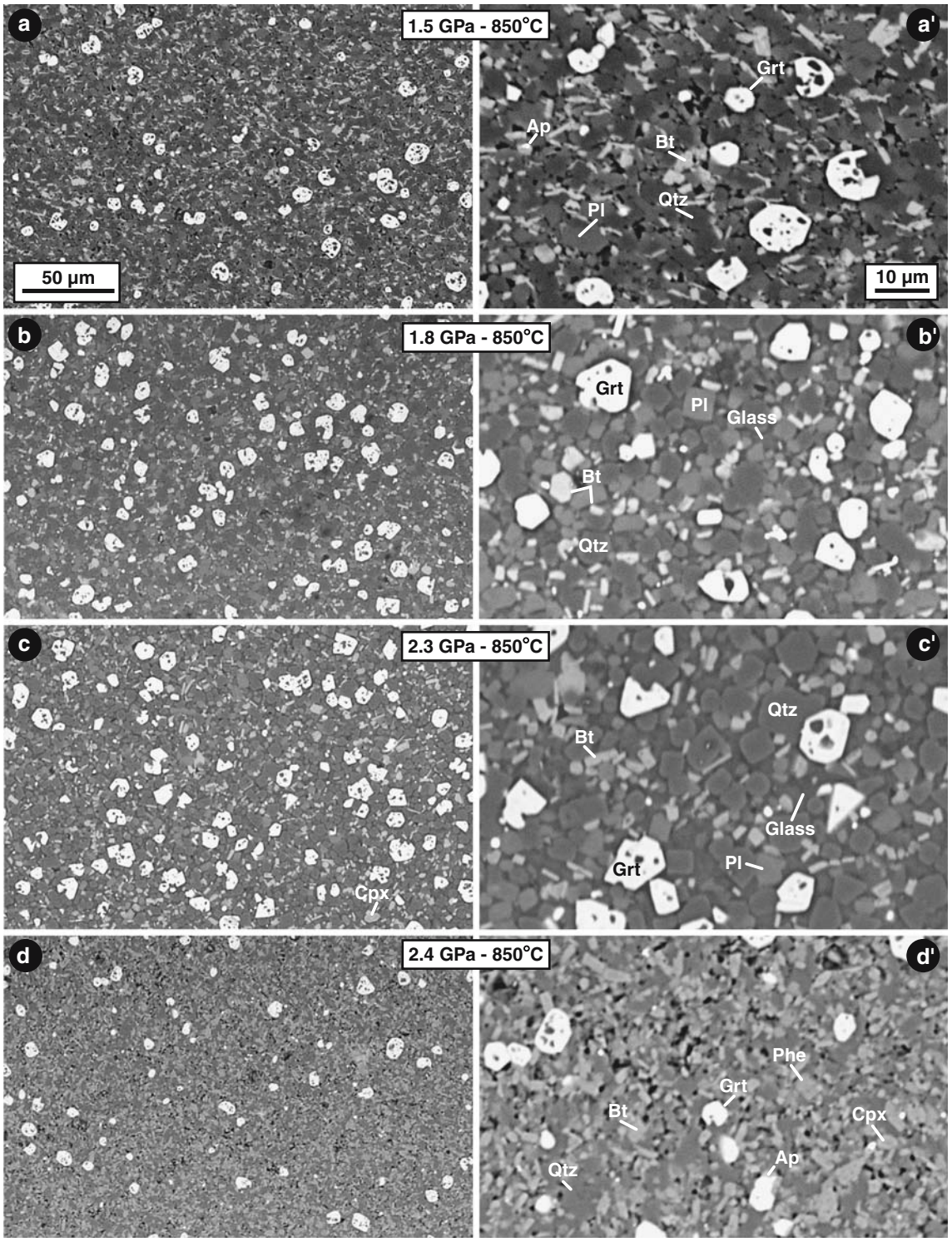

Fig. 2 BSE images of a series of melting experiments at 850°C from 1.5 to 5 GPa at two magnifications. Note the variation of the proportion of garnet and the textural changes as a function of pressure. *Black areas* in photographs **a**, **d**, **e**, **a′**, **d′**, **e′** correspond to tear offs during polishing of the sample; these are indirect indications of low melt fractions resulting in low grain coherence in the experimental charge (compare to photographs **b′** and **c′**). **f** and **f′** BSE image of a porous quartz trap in the charge at 800°C, 1.5 GPa (**f**) and detail of melt trapped in the quartz (**f′**). *Ap* apatite, *Bt* biotite, *Cpx* clinopyroxene, *Grt* garnet, *Phe* phengite, *Pl* plagioclase, *Qtz* quartz

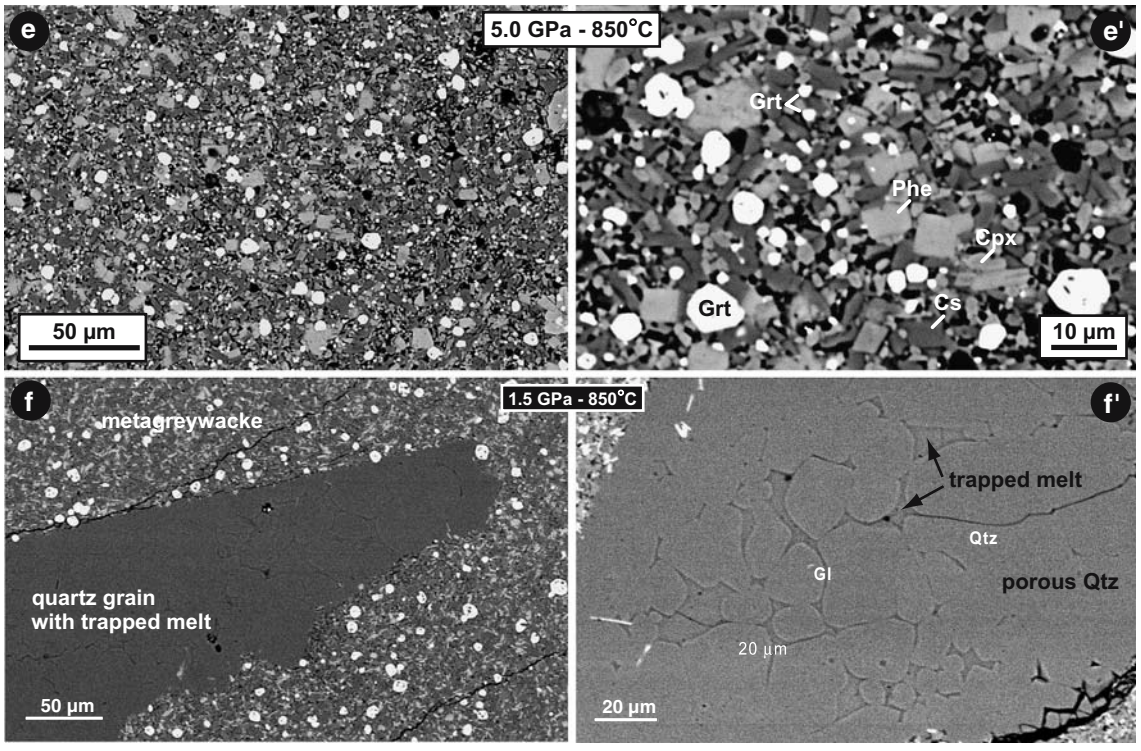

Fig. 2 continued

the melt increase is particularly sudden in the 800 and 850°C sections. This rapid increase is followed by a progressive decrease in melt proportion from 2.3 to 1.0 GPa (domain III). This latter evolution is observed in all three isothermal sections and corresponds to a melt fraction decrease of about 20% at 850 and 900°C, and 10% at 800°C. Finally, we observe a pronounced increase in melt proportion from about 10 ± 5 wt% up to 50–55 wt% from 1.0 to 0.5 GPa, both at 850 and 900°C (domain IV, Fig. 3b, c). The change in domain II coincides with the appearance of biotite and plagioclase while the transition from domains III to IV corresponds to the breakdown of biotite and the appearance of orthopyroxene.

The modal proportion of *garnet* as a function of pressure is shown in Fig. 4a–c for the three isothermal sections. The domains defined for the modal evolution of melt will be used also for garnet. In domain I, at high pressure, the modal proportion of garnet decreases progressively with decreasing pressure in all three isothermal sections. At about 2.3 GPa (domain II), a sudden increase in garnet proportion happens (5–10 wt%). This increase is more pronounced at 850 and 900°C than at 800°C. To lower pressures, in the range 2.3–1 GPa (domain III), a progressive decrease in garnet proportion (15–5 wt%) occurs. The decrease is less pronounced in the 800°C isothermal section. The melt and garnet fractions are positively correlated in domains II and III and negatively correlated in domains I and IV.

The evolution of the modal proportion of all major minerals and melt as a function of pressure and temperature are summarized in Fig. 5.

Garnet composition as a function of pressure

The variation of the garnet composition as a function of pressure is shown in Fig. 6 for the three temperature sections.

Grossular The evolution of grossular content is similar in the three isothermal sections (Fig. 6a, f, k). From 5.0 to 2.5 GPa, the molar fraction of grossular decreases slightly. This decrease is followed by a sharp increase from 0.1 to 0.2 X_{grs} within the restricted 2.5–2.3 GPa pressure range. Finally a progressive decrease of X_{grs} from 0.20 down to 0.02 is observed in the pressure range 2.3–0.5 GPa.

Almandine It is negatively correlated with the grossular content (Fig. 6b, g, l): a progressive increase from 5.0 to 2.5 GPa is followed by a sudden decrease at 2.3 GPa. This is particularly well marked in the 850°C section. Then, a new progressive increase is observed in the range 2.3–0.5 GPa. For all pres-

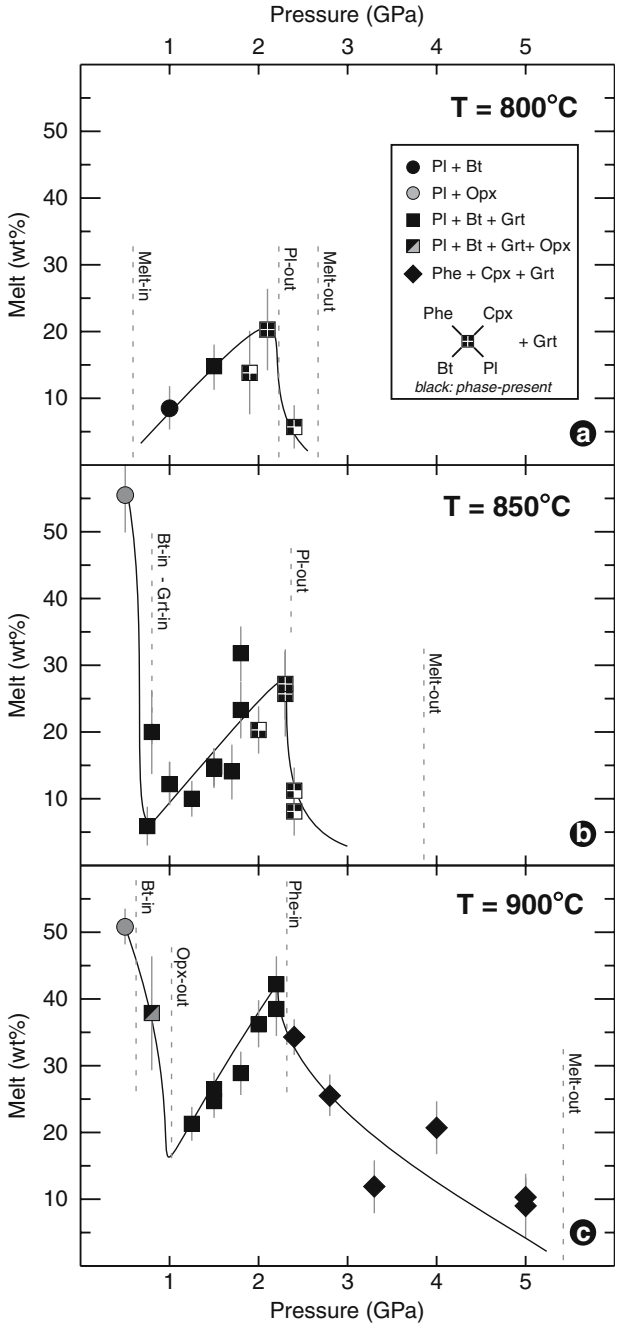

Fig. 3 Variation of the modal proportions of melt as a function of pressure at 800, 850 and 900°C. The *different symbols* are indicative of the stable mineral assemblage. *Vertical bars* plotted on the graphs are standard errors for modal proportions. *Black lines* correspond to interpretative visual best fits. Note the rapid increase of melt fraction with decreasing pressure at 2.5–2.0 GPa which corresponds to the transition from a phengite + clinopyroxene to a biotite + plagioclase assemblage

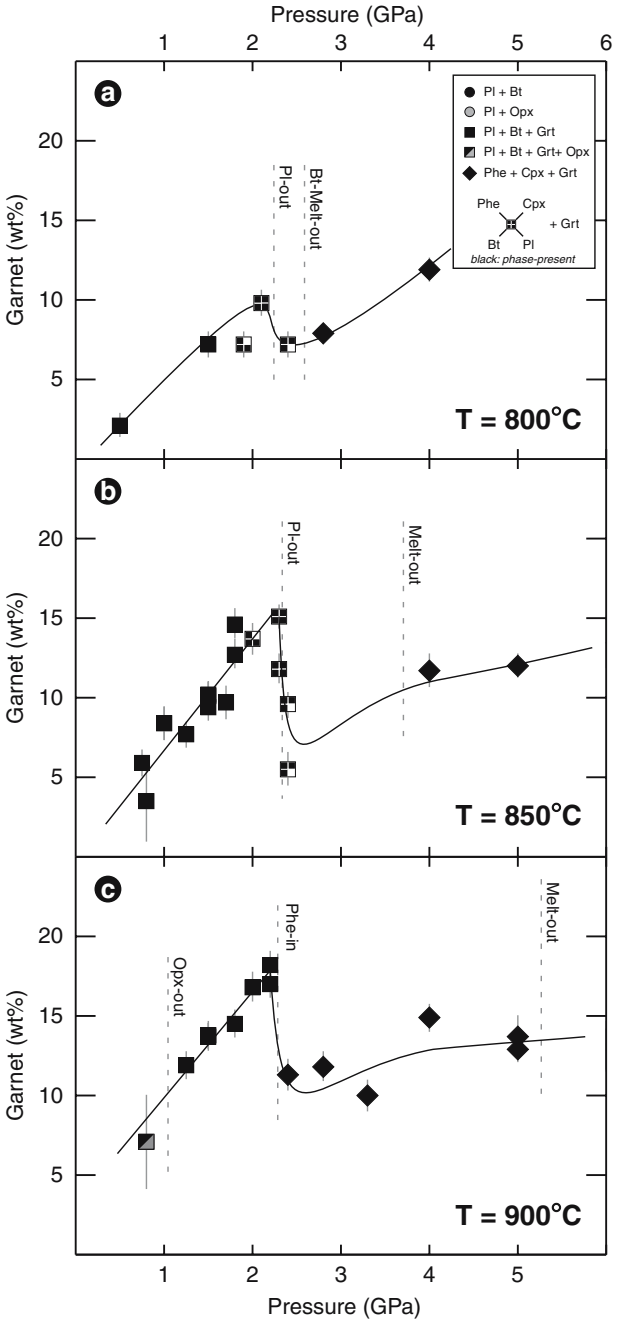

Fig. 4 Variation of the modal proportion of garnet as a function of pressure at 800, 850 and 900°C. Same symbols as in Fig. 3. The *different symbols* are indicative of the stable mineral assemblage. *Black lines* correspond to interpretative visual best fits. Note the rapid increase of garnet fraction with decreasing pressure at 2.5–2.0 GPa which corresponds to the transition from a phengite + clinopyroxene to a biotite + plagioclase assemblage

sures below 2.3 GPa, X_{alm} decreases regularly with increasing temperature at constant pressure.

Pyrope The evolution of the molar proportion of pyrope is not as dramatic as for grossular or almandine (Fig. 6c, h, m). No consistent scheme among the three isothermal sections appears in the range 5–2.3 GPa. The sharp step observed for X_{alm} at 2.5–2.3 GPa is noticeably absent in the X_{prp} trends in all temperature sections. A small and progressive increase in pyrope content happens between 2.5 and

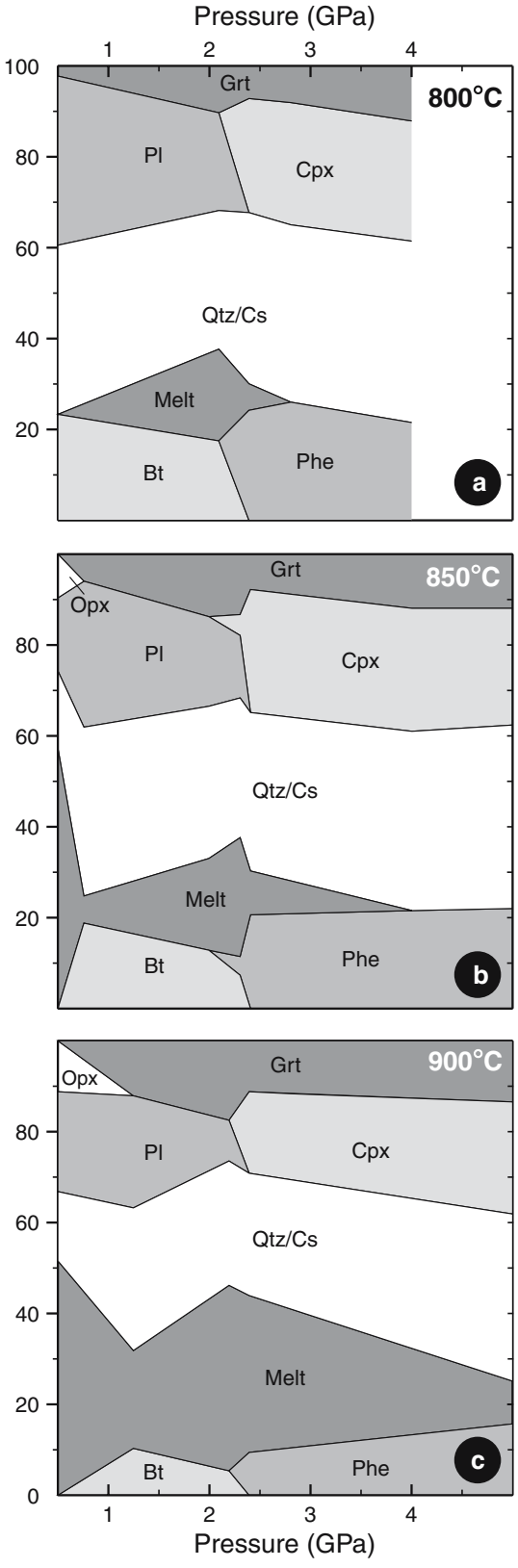

Fig. 5 Calculated phase proportions in the metagreywacke composition as a function of pressure at three different temperatures (800, 850 and 900°C)

0.5 GPa. For pressures below 2.5 GPa, X_{prp} increases regularly with increasing temperature at a constant pressure. This is not the case above 2.5 GPa.

Spessartine Figure 6d, i and n indicate that in the temperature range 800–850°C, the spessartine content of garnet decreases with both increasing pressure and temperature. At 900°C, the Mn content of the garnet is very low over the entire pressure range. No major change happens in the 2–2.5 GPa pressure interval.

X_{Fe} does not vary much with pressure above and below 2.5–3 GPa at a constant temperature. However a sudden change happens within this critical pressure range. At 800 and 850°, X_{Fe} in garnet at high pressure is lower than at low pressure, and conversely at 900°C. In other words, above 2.5–3 GPa, X_{Fe} in garnet stays almost constant over the investigated temperature range ($X_{Fe} \approx 0.65$–0.70). In contrast, below 2.3 GPa X_{Fe} changes progressively with temperature, ($X_{Fe} = 0.75$ at 800°C and 0.60 at 900°C). We ascribe this inversion to the fact that the Fe/Fe + Mg ratio in garnet is dominated by an exchange reaction with biotite at low pressure and with clinopyroxene at high pressure.

Melt composition

The silicate melts have chemical compositions corresponding to slightly peraluminous leucogranites with an alumina saturation index (Zen 1986) between 0.93 and 1.39. These melts are rich in SiO_2 (67.2–72.5 wt%), Al_2O_3 (12.1–16.5 wt%), K_2O (3.4–7.6 wt%), and Na_2O (2.1–5.4 wt%), but poor in FeO (≤ 1.0 wt%), MgO (≤ 0.4 wt%), MnO (≤ 0.1 wt%), CaO (≤ 0.8 wt%), and TiO_2 (≤ 0.3 wt%). The transition from high to low pressure mineral assemblages is not associated with a marked change in composition of the melt. In the range 2.5–0.5 GPa, the composition of the melts changes with pressure, the proportion of normative quartz increases (from 20 to 35%) while normative albite decreases from 45 to 25%. Representative compositions of melts obtained in the range 2.2–2.4 GPa are given in Table 2.

Interpretation

High pressure assemblages

Above 2.3–2.5 GPa and up to 5 GPa, the phase assemblage is simple and consists in Phe + Cpx + Grt + Qtz/Cs together with either fluid or melt. At subsolidus conditions, the starting material with

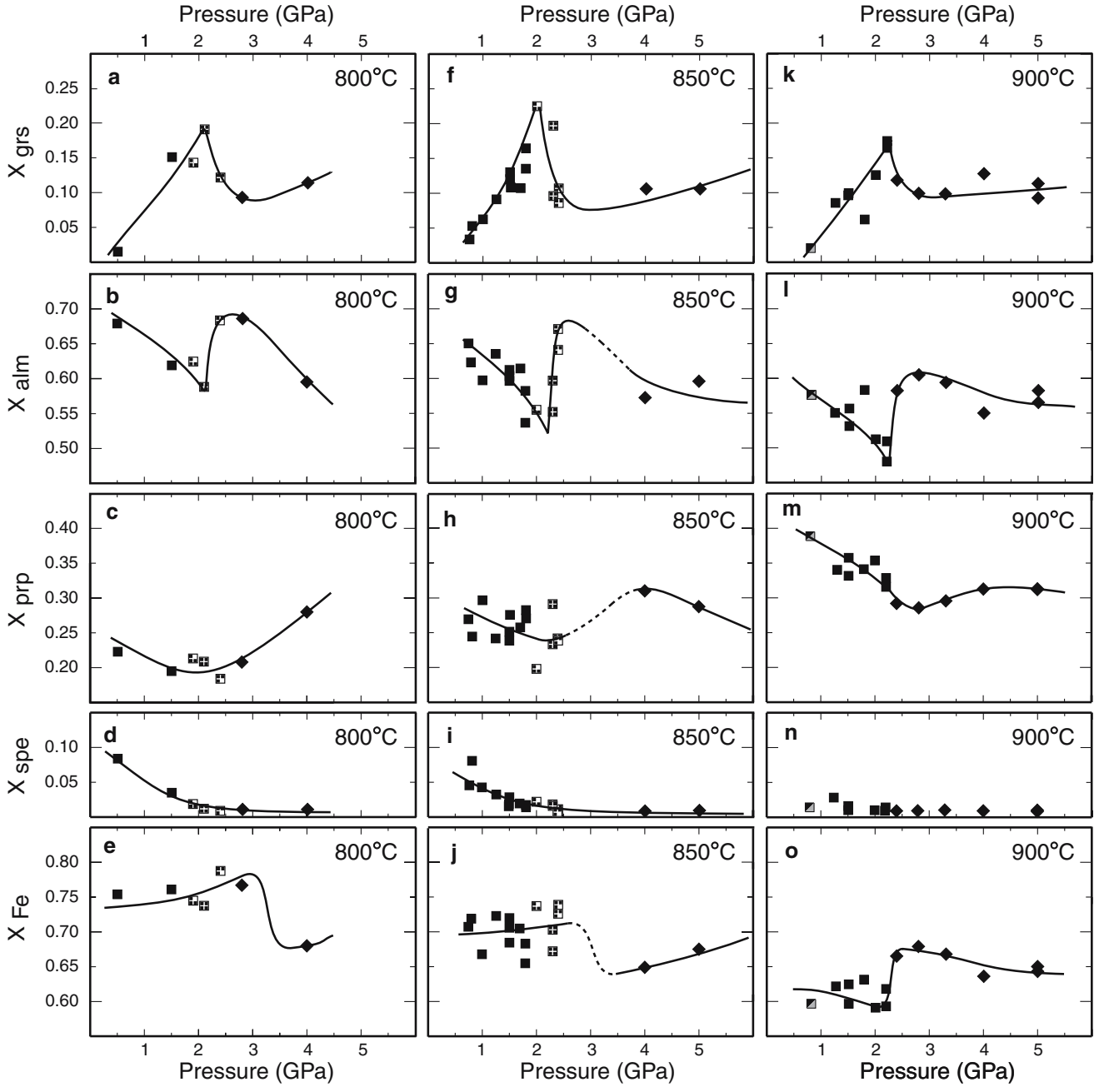

Fig. 6 Compositions of garnet between 0.5 and 5 GPa at 800, 850 and 900°C. Same symbols as in Fig. 2. Note the rapid increase of grossular component and decrease of almandine component with decreasing pressure at 2.5–2.0 GPa which corresponds to the transition from a phengite + clinopyroxene to a biotite + plagioclase assemblage

1.43 wt% H_2O in the bulk has about 0.4 wt% H_2O unbound in phengite at pressures above 2.5 GPa. Thus, at high pressure, the solidus determined in our experiments corresponds to a fluid saturated melting reaction:

$$\text{Phe} + \text{Cpx} + \text{Fl} + \text{Cs/Qtz} = \text{melt}. \quad (1)$$

As already noted by Schmidt et al. (2004), the role of garnet in this reaction is ambiguous. Garnet, a product at 5 GPa, could be involved as a reactant at relatively low pressures. This may result from the presence of a singular point along the solidus, analogous to the one defined for the basalt–H_2O system at approximately 4.5 GPa (Kessel et al. 2005, their Fig. 8). Reaction 1 indicates that some melt is expected to be produced when the fluid saturated solidus is intersected. Considering the amount of elements dissolved in the fluid phase at such pressures (Schmidt

et al. 2004), the activity of H_2O in the fluid must be reduced (Philippot 1993).

As pressure decreases from 5 to 2.3 GPa, the proportion of melt increases significantly at 900°C (Fig. 3c), while the proportion of garnet (Fig. 4a–c) decreases slowly. Reaction 2 with melt on the low pressure side is consistent with these changes (Fig. 7):

$$\text{Phe} + \text{Cpx} + \text{Grt} + \text{Qtz/Cs} = \text{melt}. \quad (2)$$

In contrast, a temperature increase at constant pressure causes a concomitant increase of modal garnet and melt, placing garnet at the opposite side of the above reaction. This contrasting evolution of the garnet/melt ratio results from the different behavior of the garnet components as a function of pressure and temperature: the grossular component decreases with decreasing pressure, while the pyrope component increases with temperature (Figs. 4, 6).

Intermediate pressure assemblages

For the studied composition, the transition from a typical eclogite facies assemblage (Phe + Cpx + Grt + Qtz/Cs) to an upper amphibolite facies assemblage (Bt + Pl + Qtz + Grt) occurs at about 2.1 GPa at 800°C and 2.3 GPa at 900°C. The overall reaction:

$$\text{Cpx} + \text{Phe} + \text{Qtz} = \text{Bt} + \text{Pl} + \text{Grt} + \text{melt} \quad (3)$$

accounts for these observations. This reaction has a slightly positive dP/dT slope and Cpx + Phe + Qtz is on the high pressure/low temperature side (Fig. 7). Its multivariant field marked by the appearance of plagioclase and the disappearance of clinopyroxene is about 0.4 GPa wide at 850°C. This reaction is consistent with the disappearance of omphacite and phengite and the appearance of biotite and plagioclase with decreasing pressure. It is also consistent with the sudden increase of melt and garnet proportions when pressure decreases from about 2.5–2.0 GPa. The most surprising fact is the presence of garnet and melt on the low pressure side of reaction 3 but this is well constrained by our data (compare Fig. 2d, c for the proportion of garnet, Fig. 2d′, c′ for the proportion of melt, and see Figs. 3, 4, 5).

Balancing reaction 3 is a necessary condition to test our model. It provides constraints on the phase assemblage that may be present in a rock after completion of the reaction. The choice of phase compositions for the calculation by a least square method is straightforward for biotite, plagioclase, clinopyroxene and phengite since these phases are present either at high pressure or low pressure. We selected a representative composition of each of these minerals in the pressure range 2.0–2.4 GPa at 850°C (Table 2). Since the composition of the melt (present in our run products at both high and low pressures) does not change significantly in the pressure range considered, we assumed that the partial melt formed by reaction 3 is

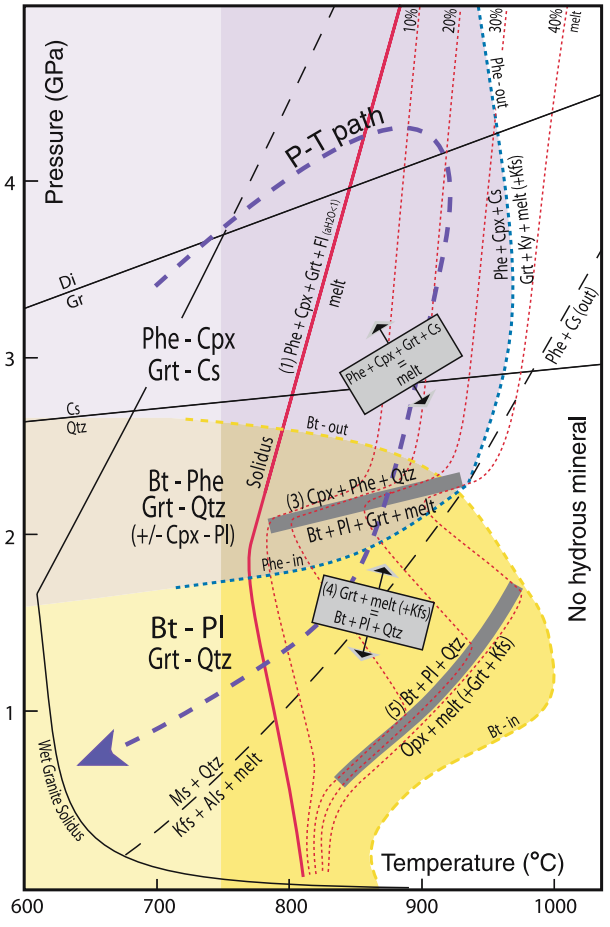

Fig. 7 Interpretative pressure–temperature diagram and location of the major melting reactions (*thick grey lines*). *Shaded rectangles with arrows* indicate reactions with wide multivariant fields. Bt-out and Phe-in lines are reported together with the solidus for the studied composition. *Red dashed lines* correspond to lines of isocontent of melt (note their zigzag shape). The *purple and yellow* areas correspond to the stability fields of phengite and biotite, respectively (note the overlap). The *white area* corresponds to the P–T domain where no hydrous mineral is stable. The *dark blue arrow* is a hypothetical P–T path for a subducted/exhumed continental crust (e.g. Kokchetav massif). Wet granite solidus after Huang and Wyllie (1973); reaction Ms + Qtz = Kfs + Als + melt after Storre (1972); Phe + Cs (out) line extrapolated from Ono (1998); reaction Cs = Qtz after Hemingway et al. (1998); reaction Di = Gr after Kennedy and Kennedy (1976). Below 800°C (*light area*), the amphibolite–eclogite facies transition may be complicated by additional hydrous phases e.g. zoisite, amphibole, paragonite, staurolite, choritoid (Schmidt and Poli 1998)

identical to the measured composition of the melt in this domain. The problem is more complex with garnet since (a) this mineral is present in our experiments at both low and high pressures and (b) its composition changes with pressure. To determine the composition of the garnet formed during reaction 3, we plotted the garnet compositions at the transition between high and low pressure assemblages in the almandine–pyrope–grossular triangle. The intersection of the extension of the tie line joining the garnets with the edge of the triangle provides the components of the garnet formed during reaction 3. The average component composition obtained using the 800°C isothermal section is $grs_{75}prp_{25}$ (SiO_2: 41.2, Al_2O_3: 23.3, MgO: 7.5, CaO: 28.0 wt%). This suggests that the total amount of almandine remains unchanged across the reaction, but that the almandine content of the newly formed garnet decreases simply by dilution. The strategy consisting in

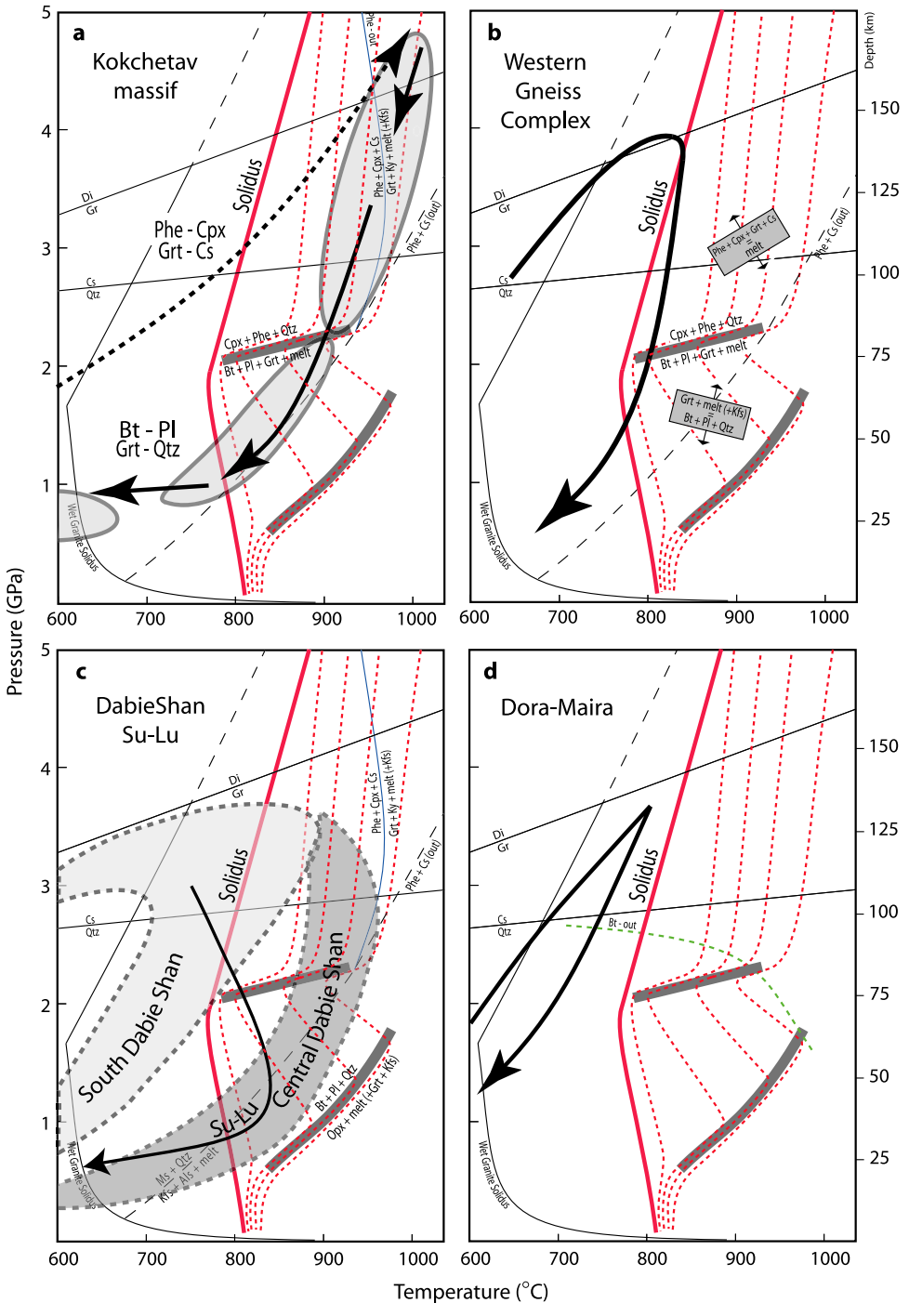

Fig. 8 Application to UHP metamorphic domains. **a** P–T path for the Kokchetav massif (Hermann et al. 2001; Dobretsov and Shatsky 2004). The *three shaded areas* correspond to domains 2, 3 and 4 defined by Hermann et al. (2001) on the basis of mineral inclusions and trace element characteristics in zircons. **b** P–T path for UHP rocks from the Moldefjord area (Nordøyane) in the northern part of the Western Gneiss Complex of Norway (Terry et al. 2000a). **c** P–T path envelopes for different UHP areas in Eastern China: *light grey*: South Dabie Shan, *dark grey* Central Dabie Shan (compiled by Faure et al. 2003). The *black arrow* corresponds to a P–T path determined by Wang et al. (1993) in the Su-Lu area where UHP assemblages are overprinted by granulite facies metamorphism. **d** P–T path for the Dora Maira UHP rocks (Schertl et al. 1991)

employing a 2-component garnet is equivalent of using two actual compositions of the garnets as formed in our experiments on each side of the reaction, but allows isolating the reactive garnet components.

Taking into consideration these constraints, reaction 3 balances as follows (in wt%):

$$45.0\,\mathrm{Phe} + 49.9\,\mathrm{Cpx} + 5.1\,\mathrm{Qtz} + 0.0\,\mathrm{Ru} = 35.7\,\mathrm{Bt} + 42.2\,\mathrm{Pl} + 5.0\,\mathrm{Grt}_{(\mathrm{grs-prp})} + 17.2\,\mathrm{melt}.$$

We tested the sensitivity of this model reaction by changing the compositions of the minerals. The values of the stoichiometric coefficients remain stable for biotite, plagioclase, phengite and clinopyroxene while the stoichiometric coefficients of garnet, melt and quartz are more sensitive to slight changes in mineral compositions. Nevertheless the estimated garnet and melt proportions produced by this reaction during decompression are in good agreement with the measurements (Figs. 3, 4). The calculation indicates that quartz is on the left hand side (HP side) of the reaction and that rutile (taken into account in our mass balance calculation) is neither consumed nor produced by reaction 3.

Low pressure assemblages

At pressures below the transition domain II and outside the stability field of orthopyroxene, most features observed in our experiments are best explained by the following reaction[2]:

$$\mathrm{Grt}_{(\mathrm{alm-prp-grs})} + \mathrm{melt}(+\mathrm{Kfs}) = \mathrm{Bt} + \mathrm{Pl}_{(\mathrm{an})} + \mathrm{Qtz}. \quad (4)$$

This reaction corresponds to a wide pressure-dependent multivariant field with Bt + Pl + Qtz on the low pressure side (Fig. 7; Vielzeuf and Montel 1994; Vielzeuf and Schmidt 2001). It is consistent with the decrease of the modal proportions of melt and garnet from 2.3 to 1.0 GPa, together with the progressive decrease of grossular content in the garnet. In this reaction, K-feldspar is a product; however, as discussed by Vielzeuf and Montel (1994), K-feldspar may not be observed as a separate phase until saturation of plagioclase in orthoclase component is reached. Reaction 4 also helps understanding why melt and garnet are found on the low pressure side of reaction 3. Indeed, as a result of reaction 4, biotite and the anorthite component in the plagioclase react with increasing pressure to form garnet and melt. Depending on the initial proportion of phases, such a process may end up with most of the calcium bound in garnet (at about 2 GPa). Thus, to higher pressure, partial breakdown of garnet is required to form the diopside component in omphacitic clinopyroxene.

Phases relationships at low pressure and high temperature (900°C) and the appearance of orthopyroxene are best interpreted through the reaction:

$$\mathrm{Bt} + \mathrm{Pl}_{(\mathrm{ab})} + \mathrm{Qtz} = \mathrm{Opx} + \mathrm{Kfs} + \mathrm{melt}\left(\pm\mathrm{Grt}_{(\mathrm{alm-prp})}\right). \quad (5)$$

The location of this mostly temperature-dependent reaction in the P–T diagram (Fig. 7), with Bt + Pl + Qtz on the low temperature/high pressure side, together with its main features have been discussed in detail by Vielzeuf and Montel (1994) and Montel and Vielzeuf (1997). In the present study, this reaction and its positive dP/dT slope are consistent with the disappearance of biotite, the crystallization of orthopyroxene and the production of a large quantity of melt with decreasing pressure at high temperature (Fig. 3b, c). The status of garnet in this reaction remains unclear. When this reaction is intersected with decreasing pressure at constant temperature, an increase in modal proportion of garnet is not observed (Fig. 4c). This is due to various reasons: (1) garnet is not required to balance the reaction when orthopyroxene is rich in alumina (Montel and Vielzeuf 1997); (2) other partial equilibria involving anorthite and grossular have a predominant effect and decrease the proportion of garnet with decreasing pressure (Vielzeuf and Montel 1994). From these observations, we conclude that garnet is not always required on the right hand side of this reaction and that reaction 5 is not critical for the presence or absence of garnet in metagreywackes. A pressure–temperature diagram summarizing the location of reactions 1–5 is shown in Fig. 7.

Discussion

The eclogite/amphibolite facies transition in felsic rocks

Reaction 3 is a model reaction of major importance as it allows the transition from eclogite- to amphibolite-facies assemblages in felsic rocks devoid of aluminum silicate. It is located at about 2.3 ± 0.2 GPa in the temperature range 800–900°C. It confirms the fact that

[2] Most minerals involved in this study are complex solid-solutions; the subscripts in the mineral abbreviations are used to indicate the main end member implied in the reaction.

Bt + Pl plays a major role in this transition below and above the solidus. This was suggested earlier by Godard (1988) who attributed the breakdown of phengite and omphacite to the reaction Cpx + Phe = Bt + Pl + Qtz in retrogressed eclogites from the Hercynian belt (see also Palmeri et al. 2003). Indeed, the formation of Bt + Pl coronas around phengite is a common feature in most retrogressed eclogitic gneisses (Heinrich 1982; Zhang et al. 2000).

Location of the solidus

The location of the solidus is important for geological applications but is difficult to determine experimentally as low melt fractions cannot be easily detected. For this purpose, the new technique of entrapment of melt in a porous quartz proved efficient. The location of the solidus for the CEV composition is shown in Fig. 7. It neither coincides with the H_2O-saturated solidus as determined by Huang and Wyllie (1973) for a synthetic granite + 30 wt% H_2O, nor with the complete breakdown of phengite or biotite. As mentioned earlier, we consider that about 0.4 wt% H_2O was set free as a fluid from the starting material at high pressures just below the solidus. In such a phase, the activity of water is reduced by (1) the presence of other fluid components such as CO_2 and N_2 (the air enclosed in the capsule), (2) dissolved elements such as Si and K (Schmidt et al. 2004), (3) other minor or trace elements present in the natural bulk composition, strongly partitioning into the fluid (e.g. Cs, Rb, Ba, Sr, B, Cl). As a result, our solidus corresponds to a fluid-present melting reaction with a reduced activity of H_2O in the fluid-phase (reaction 1). It is located between the wet solidus (with a large excess of H_2O) and the fluid-absent solidus. The exact position of such a solidus depends on the ratio of free H_2O and highly soluble minor or trace components.

Evidences of a reduced H_2O-activity in the fluids present in natural UHP rocks are common. Multiple generations of primary CO_2- or H_2O-rich fluid inclusions are reported in various minerals from the UHP Dabie Shan metamorphic terranes (Xiao et al. 2000). In the Alps, Philippot et al. (1995) report several generations of fluid-inclusions depending on the host mineral and rock type: a low salinity H_2O–CO_2 fluid, CO_2-rich fluids coexisting with brines, and a low-salinity aqueous phase. This is evidence for a limited fluid mobility, a short range equilibration and a locally reduced activity of H_2O in the fluid-phase. These observations support the presence of a fluid-phase during UHP peak metamorphism and indicate that fluid-present melting with a reduced activity of H_2O in the fluid phase may take place in eclogite facies rocks (Schreyer et al. 1987; Philippot 1993; Sharp et al. 1993).

Partial melting involving phengite will proceed immediately above the solidus. In many cases, reactions such as Ms + Qtz = Kfs + Als + melt or Phe + Cpx + Cs = Grt + Ky + melt do not mark the beginning of melting of Ms + Qtz or Phe + Cpx + Cs but rather the upper stability limit of these assemblages (Vielzeuf and Schmidt 2001). For many bulk compositions, these 'univariant' reactions do not need to be crossed for phengite melting to proceed. According to our results, temperatures of about 800°C are sufficient to promote a low but significant melt fraction in metagreywacke compositions. Thus, the influx of H_2O-rich fluids is not required to induce partial melting of the subducted continental crust.

Previous experiments indicate that critical phenomena in fluid-melt systems change melting relations at high pressure. The critical end-point of the solidus is located at about 6 GPa for this metagreywacke composition (Schmidt et al. 2004). There, the fluid-saturated solidus terminates but the melt-fluid critical curve does not affect the fluid-absent solidus which continues to higher pressures. Thus, beyond 6 GPa, our melting model would be modified in terms of deep fluid or melt phases but the general geological relationships would remain unchanged.

Decompression melting and zigzag shape of isotects

The presence of melt on the low pressure side of reaction 3 characterized by a relatively small dP/dT slope is a fact of major importance. It implies a sudden increase in the proportion of melt in felsic rocks at about 2.3 GPa during decompression if sufficiently high temperatures are reached during the thermobaric history. In Fig. 7, isotects (lines of constant proportion of melt) have been reported on the basis of our experimental results. Low pressure isotects are modified from Montel and Vielzeuf (1997). Figure 7 shows that, as to be expected but rarely demonstrated, both the spacing and the slope of the isotects change as a function of P and T, and depend on the melting reaction involved. Note that major perturbations occur in the vicinity of reactions 3 and 5. Thus, the succession of melting reactions is responsible for the zigzag shape of the isotects. Along a typical P–T path for UHP metamorphic rocks as shown in Fig. 7, the proportion of melt is expected to increase from the solidus up to the maximum temperature reached during the prograde path. Upon decompression, the proportion of melt is expected to remain constant or to slowly decrease until 2.3 GPa. There, a significant additional proportion of

melt (10–15%) will form upon the breakdown of clinopyroxene and phengite. Below 2.3 GPa, the proportion of melt should decrease progressively with pressure until the solidus is reached, melt and garnet reacting to form additional biotite and plagioclase.

Since the melt phase may escape or has to recrystallize upon cooling, melting stages are difficult to record and recognize in rocks through the melt phase itself. On the contrary, the changes in melt proportion are well recorded by garnet growth zoning.

Garnet zoning

Garnet is present almost throughout the studied P–T domain and shows significant chemical changes as a function of both pressure and temperature. Considering the same P–T path as above, a general pattern for garnets present along this path can be proposed for greywacke compositions. Above the solidus, the proportion of garnet is not expected to grow significantly during the prograde path (Fig. 4). During the first stage of decompression at high pressure, the isothermal sections indicate that the modal proportion of garnet should decrease (Fig. 4). Thus, some limited resorption of garnet crystals should happen. This stage might be registered in the garnet by dissolution features at the surface of the crystals. At about 2.3 GPa, a new growth zone (corresponding to a 5–10% increase of modal garnet) should form with a characteristic grossular-rich composition. It is important to note that Fig. 6 gives the chemical composition of homogeneous garnets in chemical equilibrium with other phases; it can only be used to approximate the composition of a garnet overgrowth resulting from reaction 3. For instance, before and after reaction 3 the bulk garnet composition should change from about Grs_{10} to Grs_{20}; (Fig. 6a, f, k). However, in nature, most of the almandine-rich core will not re-equilibrate due to slow diffusion rates (Ganguly et al. 1998) and as a consequence, the garnet overgrowth zone formed during decompression will have a grossular content much higher than Grs_{20} (the composition of the rim should be closer to the fractional garnet formed by reaction 3). Finally, to lower pressures (below 2.3 GPa), garnet + melt should progressively break down to produce Bt + Pl. Once again, such stage might be registered in the garnet only by dissolution features at the surface of the crystals.

Summarizing, garnets formed during a burial/exhumation cycle should show the alternation of growth zones interrupted by dissolution surfaces. Diffusive homogenization may superimpose upon the major growth features. One of the implications of this general pattern is that a grossular-rich zone may not be representative of the highest pressures reached along the P–T path. In order to recognize grossular-rich zones indicative of metamorphic climax in the subsolidus at high pressure and those formed by partial melting during decompression, the combination of major and trace element distributions may prove effective. Further evidence that grossular-rich zones in garnet coexisted with melt during their formation may stem from the partitioning behavior of HREE and Y between melt and garnet. Experimental studies indicate that phosphate minerals readily dissolve in peraluminous melts such as those formed in our experiments (Pichavant et al. 1992; Montel 1993). In the absence of phosphates, garnet and zircon are the phases preferentially incorporating Y and HREE (Pyle and Spear 2003; Bea et al. 1994). A positive correlation between Ca, and Y and/or HREE would thus point to growth of grossular-rich zones in the presence of melt and constitute a useful geodynamic indicator for decompression melting.

The prediction that the grossular content of garnet may increase during decompression is in disagreement with previous experiments carried out by Hermann and Green (2001) and Hermann (2002). In these experiments, the grossular content of garnet increases monotonously with pressure from 2 to 4.5 GPa (Hermann and Green 2001, their Fig. 4). A reason of this apparent discrepancy is that the experiments of Hermann and Green were carried out in a synthetic KCMASH system not allowing the presence of sodic plagioclase at low pressure nor the presence of jadeite component in clinopyroxene at high pressure. Our data in a natural system involving Na show that the grossular content of garnet is strongly dependent on the nature and composition of the coexisting calcic phases (plagioclase at low pressure and clinopyroxene at high pressure), both closely linked to the Na component. Rather than contradicting the study of Hermann (2002), our data complement it towards a direct applicability to natural bulk compositions.

Evidences of decompression melting in UHP domains

Diamondiferous rocks representing deeply subducted continental crust are observed in the *Kokchetav Massif*, Kazakhstan (Sobolev and Shatsky 1990; Dobretsov and Shatsky 2004). The peak metamorphic conditions (4.5 GPa, 950°C) and the P–T path (Fig. 8a) imply partial melting at some stage of the evolution (Shatsky et al. 1995; Hermann et al. 2001). This interpretation is consistent with the fact that diamond-bearing gneisses are characterized by some depletion in K, Na, Si and

light rare earth elements (LREE) indicative of melt-depleted rock types (Shatsky et al. 1995, 1999; Dobretsov and Shatsky 2004). Interestingly, diamondiferous rocks are associated with migmatites in the field, and age determinations indicate similar ages for both rock types (Shatsky et al. 1999; Borisova et al. 1995). Zircons from the diamondiferous gneisses have been investigated by Hermann et al. (2001). Four different zircon growth zones have been identified by their trace element contents and mineral inclusions. Domain 1 lacks evidence of UHP metamorphism, domain 2 contains diamond, coesite, omphacite and Ti-rich phengite indicating that this zircon zone grew under UHP conditions. Domain 3 is characterized by LP mineral inclusions such as biotite and plagioclase, which, together with garnet inclusions, are indicative of an upper amphibolite/granulite-facies overprint. According to Hermann et al. (2001), the multi-stage zircon growth is best explained by growth from zircon-saturated partial melts present in the gneisses. The different zircon domains were dated by SHRIMP and provided similar ages within the resolution of the instrument, indicating that decompression took place in less than 6 Ma. Our experimental results support these observations, these interpretations and the presence of a melt throughout the retrogression of these rocks at HP. They allow a tighter P–T location for the transition between domains 2 and 3 (2.3 ± 0.2 GPa). Interestingly, garnet zoning in the gneisses is generally characterized by an increase in Ca content from core to rim (Shatsky et al. 1995; Hermann et al. 2001). Hermann et al. (2001) suggest that this feature is the result of the control of the grossular content of the garnet by the reaction An = Grs + Als + Qtz, and is indicative of a nearly isobaric cooling. Instead, our results suggest that reaction 3 is responsible for both the change from high pressure to low pressure assemblages and the enrichment in grossular content of the garnet towards the rim. This challenges the existence of a near isobaric cooling for these rocks at 1 GPa.

The *Western Gneiss Complex (WGC)* in Norway is a classic area of exposure of crustal rocks metamorphosed in the eclogite facies (Eskola 1921; Krogh 1977; Cuthbert et al. 2000). The discovery of coesite (Smith 1984) and microdiamonds (Dobrzhinetskaya et al. 1995) established that this region (at least parts of it) attained UHP conditions during its geological history. From geothermobarometric studies on phengite-bearing eclogites, Cuthbert et al. (2000) proposed that pressures and temperatures progressively increased from 500°C and 1.6 GPa in the South (Sunnfjord) to > 800°C and 3.2 GPa in the North (Moldefjord). Metamorphic conditions and a P–T path for the Moldefjord area (Nordøyane) are provided by Terry et al. (2000a) and reported in Fig. 8b. This P–T path is consistent with the formation of melt during the exhumation of the UHP rocks. In addition, Terry et al. (2000b) showed electron microprobe maps of Ca in a garnet from a microdiamond bearing kyanite gneiss with a clear progressive Ca increase from core to rim. In this rock, the metamorphic assemblage is interpreted as retrograde relative to original UHP conditions. Such garnets contain abundant inclusions of kyanite, quartz, biotite and plagioclase (Terry et al. 2000b) but their precise location with respect to the chemical zoning of garnet is not mentioned.

Partial melting of UHP rocks seems to have been a feature overlooked in the WGC of Norway (Labrousse et al. 2002; Cuthbert and Carswell 2004). Since anatectic migmatites are the dominant country rock enclosing the Scandian HP and UHP units, it is necessary to distinguish the pre-Scandian proterozoic migmatites from those formed during the Scandian collision/exhumation event, and from those formed during the latest stages of evolution and relaxation of the orogen.

Labrousse et al. (2002) pointed out that the main gneissic unit lithologies in the UHP province of Western Norway display a 'modest but widespread' migmatization. According to them, partial melting would be part of the exhumation history and not a late feature. Considering that the P–T path they determined is located between the H_2O-saturated and the dehydration melting curves for crustal rocks, the authors consider that low H_2O contents were representative of prograde and climax metamorphic conditions and that water–rich fluid influx occurred during exhumation. We challenge the second part of these conclusions as our experiments demonstrate that the influx of fluids is not required to generate low but significant melt fractions (10–30%) at temperatures of about 800–850°C.

Cuthbert and Carswell (2004) consider that partial melting in the UHP rocks during decompression appears to be most intense in the northern WGC (including the Moldefjord area). There, porphyroclastic mylonites preserve evidence of granitic leucosomes with restitic garnet and kyanite. Garnet zoning and inclusion patterns are consistent with the breakdown of phengite during decompression. A systematic grossular increase towards the rim is observed in the garnets from this area (Carswell et al. 2006). Our experiments are in agreement with both the occurrence of melting during decompression and the fact that only the garnet cores formed under UHP conditions.

The *Dabie Shan—Sulu area* in East-Central China is the largest UHP metamorphic terrane recognized so far. Coesite and microdiamonds have been observed as inclusions in minerals from eclogites and the surrounding gneisses (Okay et al. 1989; Wang et al. 1989; Xu et al. 1992). Different geological units with diverse exhumation histories have been characterized in this complex metamorphic belt. Two separate P–T path envelopes for the South and Central Dabie Shan units have been compiled by Faure et al. (2003). The major part of the P–T paths for the South Dabie Shan unit, where UHP parageneses are well preserved, do not intersect the solidus at 800°C (Fig. 8c). On the other hand, the P–T paths of the Central Dabie Shan unit, a migmatitic dome without UHP relicts, are well within the melting domain. This P–T envelope is well characterized at low pressure, however, its upper part relies upon the assumption that the low pressure rocks experienced the HP or UHP event before retrogression (Faure et al. 2003). P–T paths reported by Xiao et al. (2002) for the South and North Dabie Shan regions point out very high temperatures at the peak of metamorphism or during decompression (900°C, 3 GPa for South Dabie Shan; 950°C, 1 GPa for North Dabie Shan). Such temperatures imply extensive melting of the continental crust (ca. 50%) and the presence of characteristic UHT metamorphic parageneses not observed in the field. Nevertheless, it seems likely that some of the metamorphic units experienced temperatures in the range 800–850°C near 2.5 GPa and thus underwent partial melting. Only a few studies discuss the possibility of partial melting during exhumation of the UHP terranes in the Dabie Shan area. Zhong et al. (1999, 2001) and Zhang et al. (2001) consider that the foliated garnet-bearing granites, commonly found in the UHP domains, are the products of partial melting of the UHP units at an early stage of their exhumation. Indeed, U–Pb zircon dating on two foliated garnet-bearing granites in the Western Dabie Shan UHP metamorphic unit support this interpretation: zircons are concordant and indicate ages of 227 and 234 Ma within the accepted UHP peak metamorphic age interval (220–240 Ma). Since no coesite is found in the garnets of these foliated granites (but is observed in rare zircon cores), Zhang et al. (2001) consider that the foliated granites formed just after the UHP peak of metamorphism and that the magma emplacement age of 234 Ma gives the lowest limit of the UHP metamorphic event.

In the Su-Lu region, 500 km north-east of the Dabie Shan mountains, granulite facies metamorphism, superimposed upon UHP assemblages, has been reported (Wang et al. 1993; Nakamura and Hirajima 2000; Yao et al. 2000). The P–T path representative of this region (Fig. 8c) indicates that melting conditions were reached during decompression in this area. Wallis et al. (2005) determined the age of strongly deformed K-feldspar-rich dikes in the northern part of the Su-Lu terrane. The fact that the crystallization ages of the dikes overlap with the age of peak UHP metamorphic conditions is another indication of the presence of melt during metamorphism. Our data support the interpretation that partial melting may have occurred during decompression in at least some of the Dabie Shan and Su-Lu crustal units. Reaction 3 would locate the melting event at about 2.3 GPa and is consistent with the presence of garnet in the melt. Hermann (2002) concluded that isothermal decompression produced partial melting in the UHP rocks from China. However, he limited this possibility to the Su-Lu region and located the solidus at a significantly lower pressure (ca. 1.2–1.4 GPa). Here, we conclude that partial melting initiated under UHP conditions and occurred not only in the Su-Lu region but also in parts of the South Dabie Shan units.

The description of pyrope-coesite assemblages in the *Dora Maira massif*, Western Alps, provided the first indication that continental crust could be subducted to depths of at least 100 km (Chopin 1984). A variety of mineralogical and petrological studies summarized in Chopin and Schertl (2000) present a P–T path that did not exceed 800°C (Fig. 8d). Under such conditions, melting of the continental crust seems unlikely (Compagnoni and Rolfo 2000). However, in the country rocks mainly composed of biotite–phengite gneisses, Schertl et al. (1991) noted the presence of quartzo-feldpathic veins of a ''metatectic'' character indicative of the beginning of melting at some stage during the metamorphic history of these rocks. An activity of H_2O slightly higher than the one in our experiments would lower the solidus by a few tens of degrees and allow the Dora Maira P–T path to intersect the solidus (Schreyer et al. 1987; Philippot 1993; Sharp et al. 1993). In the biotite-phengite gneisses, Schertl et al. (1991) observed different types of garnet: some inclusions of garnet in plagioclase are rich in grossular (Grs_{85}) while garnets in the matrix are poorer ($Grs_{52\text{-}44}$). In addition, Chopin and Schertl (2000) and Nowlan et al. (2000, their Fig. 9) noted a systematic increase of grossular content in the outermost uncorroded rims of garnet. Our experimental study provides an explanation for these features which are consistent either with the implication of reaction 3, i.e. melting during exhumation, or with a subsolidus equivalent of reaction 3 during retrogression.

Melting in felsic versus melting in mafic rocks

A contrasting behavior of felsic and mafic rocks during retrogression has been underlined by Heinrich (1982). Here we discuss the contrasting behavior of these two lithologies during prograde UHP metamorphism. Reversible versus irreversible mineral assemblage transformations rely in great part upon the preservation of the initial bulk composition, especially H_2O, during the metamorphic history. Felsic and mafic rocks behave differently because phengite, a major hydrous phase in metapelites and metagreywacke, is stable to very high pressures (ca 8 GPa, Ono 1998) while amphibole and zoisite, the major hydrous minerals in mafic eclogites cease to be stable at about 2.5 and 3.0 GPa, respectively, without being replaced by another hydrous mineral at near solidus conditions (Poli 1993; Vielzeuf and Schmidt 2001 for a review). The consequence is that mafic rocks may lose their H_2O component during a prograde path to become anhydrous eclogites (+ free fluid) while metapelites and metagreywackes may not. The fate of H_2O released by the breakdown of amphibole and zoisite at high pressure (at 2.5–3.0 GPa) is not known (see Philippot 1993 for a discussion) but part of it may be held responsible for an increased activity of H_2O in the fluid phase and the initiation of partial melting at relatively low temperature in felsic and mafic compositions. Such fluids could be an explanation for the trondhjemitic veins observed in eclogites throughout the northern WGC in Norway (Cuthbert and Carswell 2004). The presence or absence of a hydrous mineral in the rock at peak metamorphic conditions and during exhumation has profound consequences on both the generation of melt and retrogression. The breakdown of phengite in metagreywackes during decompression allows a melting pulse at the eclogite/amphibolite facies transition and crystallization of biotite and plagioclase, an assemblage typical of amphibolite facies conditions without influx of a fluid. On the contrary, only an ingress of H_2O may allow the mafic dry eclogites to turn into amphibolite-facies assemblages. According to Heinrich (1982), this would be a major reason why eclogite facies mafic lenses are often found embedded in upper amphibolite facies felsic gneisses. The influx of H_2O-rich fluids is commonly invoked to generate partial melting in high pressure domains. Such a process cannot be ruled out; however we consider that a massive influx of H_2O is not very common as it would allow extensive melting and retrogression of all lithologies, including the mafic ones as the wet solidus for both rock types are remarkably close to each other. Thus, the comparison of the behavior of mafic and felsic lithologies with respect to decompression and melting may be a good indicator of the fluid regime that prevailed during the exhumation.

Conclusion

Our experimental study demonstrates that a melting pulse should happen at the eclogite/amphibolite facies transition during decompression and exhumation of the subducted continental crust. The survey of the main UHP metamorphic regions indicates that partial melting in the felsic lithologies may have played a role during the exhumation of these units. Indications of melting in the field are more obvious in the Kokchetav Massif of Kazakhstan, the Western Gneiss Complex of Norway, and the Su-Lu region in China, less obvious in the South Dabie Shan area of China, and remain to be demonstrated in the Dora Maira UHP unit, Italy. A striking feature of the UHP felsic rocks that underwent retrogression is that garnet rims are commonly enriched in grossular. For most of these garnets, whether the Ca-rich zones correspond to Y and HREE enriched zones remains to be determined. Such chemical heterogeneities and their subsequent relaxation by chemical diffusion are particularly useful to determine the duration of geological events, for instance the rate of exhumation (Perchuk et al. 1999). For such studies, it is important to understand the origin of the initial zoning to specify which event is dated. In this study, we demonstrate that a high grossular content is not necessarily synonymous with the highest pressure, but that it can be representative of a very specific stage during decompression.

Acknowledgements This work is part of a PhD thesis prepared by E. Auzanneau at Université Blaise Pascal under the supervision of D.V. Experiments above 3.5 GPa were carried out in the CNRS-INSU multi-anvil national instrument at Clermont-Fd. This work has been supported by CNRS-INSU through grants DyETI 2001/021 and DyETI 2002 to D.V. We thank M. Veschambre, J-L. Devidal and F. Faure for assistance with the electron microprobe and the scanning electron microscope. J.M. Montel and R. Kryza participated in some experiments and provided some mineral analyses; they are gratefully acknowledged. We thank P. Luffi and P.J. Wyllie for some helpful comments of an early version of the manuscript and S. Harley, J. Hermann and an anonymous reviewer for their reviews.

References

Albarède F, Provost A (1977) Petrological and geochemical mass-balance equations: an algorithm for least-square fitting and general error analysis. Comput Geosci 3(2):309–326

Ancey JJ, Bastenaire F, Tixier R (1978) Application des méthodes statistiques en microanalyse. In: Maurice F, Meny L,

Tixier R (eds) Microanalyse, microscopie électronique à balayage. Les éditions des physiciens, Orsay, pp 323–347
Bea F, Pereira MD, Stroh A (1994) Mineral/leucosome trace-element partitioning in a peraluminous migmatite. A laser ablation ICP-MS study. Chem Geol 117:291–312
Borisova EY, Bibikova EV, Dobrzhinetskaya LF, Makarov VA (1995) Geochronological study of zircons from granite-gneiss from Kokchetav diamondiferous area (in Russian). Dokl Akad Nauk 343:801–805
Carswell DA, Cuthbert SJ, Massonne H-J (2006) Phengite dehydration melting in the microdiamond-bearing garnet kyanite gneisses on Fjortoft, west Norway (submitted to Lithos)
Cawthorn RG, Collerson KD (1974) The recalculation of pyroxene end-member parameters and the estimation of ferrous and ferric iron content from electron microprobe analyses. Am Mineral 59:1203–1208
Chopin C (1984) Coesite and pure pyrope in high grade blueschists of the western Alps: a first record and some consequences. Contrib Mineral Petrol 86:107–118
Chopin C, Schertl H-P (2000) The UHP unit in the Dora-Maira Massif, Western Alps. In: Ernst WG, Liou JG (eds) Ultra-high pressure metamorphism and geodynamics in collision-type orogenic belts. Geological Society of America, International Lithosphere Program, contribution No. 344, pp 133–148
Coleman RG, Wang X (1995) Ultrahigh-pressure metamorphism. Cambridge University Press, Cambridge, pp 528
Compagnoni R, Rolfo F (2000) Characteristics of UHP pelites, gneisses, and other unusual rocks. In: Ernst WG, Liou JG (eds) Ultra-high pressure metamorphism and geodynamics in collision-type orogenic belts. Geological Society of America, International Lithosphere Program, contribution No. 344, pp 74–92
Cuthbert SJ, Carswell DA (2004) Decompression melting of UHP rocks in the Western Gneiss Region of Norway. 32nd IGC Topical symposium T36, Firenze, Italy
Cuthbert SJ, Carswell DA, Krogh-Ravna EJ, Wain A (2000) Eclogites and eclogites in the Western Gneiss Region, Norwegian Caledonides. Lithos 52:165–195
Dobretsov NL, Shatsky VS (2004) Exhumation of high-pressure rocks of the Kokchetav massif: facts and models. Lithos 78:307–318
Dobrzhinetskaya LF, Eide EA, Larsen RB, Sturt BA, Trønnes RG, Smith DC, Taylor WR, Posukhova TV (1995) Microdiamond in high-grade metamorphic rocks of the Western Gneiss Region, Norway. Geology 23:597–600
Eggler DH (1973) Principles of melting of hydrous phases in silicate melt. Carnegie Inst Washington, Year Book 72:491–495
Eskola P (1921) On the eclogites of Norway. Skrifter Norske Videnskaps-Akademi Oslo. K1, I, 8, 118 pp
Faure M, Lin W, Schärer U, Shu L, Sun Y, Arnaud N (2003) Continental subduction and exhumation of UHP rocks. Structural and geochronological insights from the Dabieshan (East China). Lithos 70:213–241
Ganguly J, Cheng W, Chakraborty S (1998) Cation diffusion in aluminosilicate garnets experimental determination in pyrope-almandine diffusion couples. Contrib Mineral Petrol 131:171–180
Godard G (1988) Petrology of some eclogites in the Hercynides: the eclogites from the southern Armorican Massif, France. In: Smith DC (ed) Eclogites and eclogite-facies rocks. Elsevier, Amsterdam, pp 451–510
Heinrich CA (1982) Kyanite–eclogite to amphibolite facies evolution of hydrous mafic and politic rocks, Adula nappe, Central Alps. Contrib Mineral Petrol 81:30–38
Hemingway BS, Bohlen SR, Hankins WB, Westrum EFJ, Kuskov OL (1998) Heat capacity and thermodynamic properties for coesite and jadeite, reexamination of the quartz-coesite equilibrium boundary. Am Mineral 83:409–418
Hermann J (2002) Experimental constraints on phase relations in subducted continental crust. Contrib Mineral Petrol 143:219–235
Hermann J, Green DH (2001) Experimental constraints on high pressure melting in subducted crust. Earth Planet Sci Lett 188:149–168
Hermann J, Rubatto D, Korsakov A, Shatsky VS (2001) Multiple zircon growth during fast exhumation of diamondiferous deeply subducted continental crust (Kokchetav Massif, Kazakhstan). Contrib Mineral Petrol 141:66–82
Huang WL, Wyllie PJ (1973) Melting relations of muscovite–granite to 35 kbar as a model for fusion of metamorphosed subducted oceanic sediments. Contrib Mineral Petrol 42:1–14
Kadik AA, Frenkel MY (1980) Magma formation associated with decompression of crust and mantle rocks in the presence of volatile components. Geochem Int 17(2):77–101
Kennedy CS, Kennedy GC (1976) The equilibrium boundary between graphite and diamond. J Geophys Res 81:2467–2470
Kessel R, Ulmer P, Pettke T, Schmidt MW, Thompson AB (2005) The water–basalt system at 4 to 6 GPa: Phase relations and second critical endpoint in a K-free eclogite at 700 to 1400°C. Earth Planet Sci Lett 237:873–892
Krogh EJ (1977) Evidence of Precambrian continent–continent collision in western Norway. Nature 267:17–19
Labrousse L, Jolivet L, Agard P, Hébert R, Andersen TB (2002) Crustal-scale boudinage and migmatization of gneiss during their exhumation in the UHP province of Western Norway. Terra Nova 14(4):263–270
Montel J-M (1993) A model for monazite/melt equilibrium and application to the generation of granitic magmas. Chem Geol 110:127–146
Montel J-M, Vielzeuf D (1997) Partial melting of metagreywackes. Part II Compositions of minerals and melts. Contrib Mineral Petrol 128:176–196
Nakamura D, Hirajima T (2000) Granulite-facies overprinting of ultrahigh-pressure metamorphic rocks, northern Su-Lu region, eastern China. J Petrol 41:563–582
Nowlan EU, Shertl H-P, Schreyer W (2000) Garnet–omphacite–phengite thermobarometry og eclogites from the coesite-bearing unit of the southern Dora-Maira Massif, Western alps. Lithos 52:197–214
Okay AI, Xu ST, Sengor AMC (1989) Coesite from the Dabie Shan eclogites central China. Eur J Mineral 1:595–598
Ono S (1998) Stability limits of hydrous minerals in sediment and mid-ocean ridge basalt compositions: implications fro water transport in subduction zones. J Geophys Res 103:18253–18267
Palmeri R, Ghiribelli B, Talarico F, Ricci CA (2003) Ultra-high-pressure metamorphism in felsic rocks: the garnet–phengite gneisses and quartzites from the Lanterman Range, Antartica. Eur J Mineral 15:513–525
Patiño Douce AE (2005) Vapor-absent melting of tonalite at 15–32 kbar. J Petrol 46:275–290
Patiño Douce AE, McCarthy TC (1998) Melting of crustal rocks during continental collision and subduction. In: Hacker BR,

Liou JG (eds) When continents collide: geodynamics and geochemistry of ultrahigh-pressure rocks. Kluwer, Dordrecht, pp 27–55
Perchuk A, Philippot P, Erdmer P, Fialin M (1999) Rates of thermal equilibration at the onset of subduction deduced from diffusion modeling of eclogitic garnets, Yukon-Tanana terrane, Canada. Geology 27:531–534
Pettijohn FJ (1963) Data of geochemistry, chap. S., chemical composition of sandstones—excluding carbonate and volcanic sands. US Geol Surv Prof Pap 440-S, 21 p
Philippot P (1993) Fluid-melt-rock interaction in mafic eclogites and coesite-bearing metasediments: constraints on volatile recycling during subduction. Chem Geol 108:93–112
Philippot P, Chevallier P, Chopin C, Dubessy J (1995) Fluid composition and evolution in coesite-bearing rocks (Dora-Maira massif, Western Alps): Implications for element recycling during subduction. Contrib Mineral Petrol 121:29–44
Pichavant M, Montel J-M, Richard LR (1992) Apatite solubility in peraluminous liquids—experimental data and an extension to the Harrison-Watson model. Geochim Cosmochim Acta 56:3855–3861
Poli S (1993) The amphibolite-eclogite transformation; an experimental study on basalt. Am J Sci 293:1061–1107
Pyle JM, Spear FS (2003) Yttrium zoning in garnet: coupling of major and accessory phases during metamorphic reactions. Am Mineral 88:708
Schertl H-P, Schreyer W, Chopin C (1991) The pyrope–coesite rocks and their country rocks at Parigi, Dora Maira Massif, Western Alps: detailed petrography, mineral chemistry and PT-path. Contrib Mineral Petrol 108:1–21
Schmidt MW, Poli S (1998) Experimentally based water budgets for dehydrating slabs and consequences for arc magma generation. Earth Planet Sci Lett 163:361–379
Schmidt MW, Vielzeuf D, Auzanneau E (2004) Melting and dissolution of subducting crust at high pressures: the key role of white mica. Earth Planet Sci Lett 228:65–84
Schreyer W, Massonne H-J, Chopin C (1987) Continental crust subducted to mantle depths near 100 km: implications for magma and fluid genesis in collision zones. In: Mysen B (ed) Magmatic processes: physico-chemical principles: the Geochem Soc Spec Publ 1:155–163
Sharp ZD, Essene EJ, Hunziker JC (1993) Stable isotope geochemistry and phase equilibria of coesite-bearing whiteschists, Dora Maira massif, western Alps. Contrib Mineral Petrol 114:1–12
Shatsky VS, Sobolev NV, Varilov MA (1995) Diamond bearing metamorphic rocks of the Kokchetav Massif (northern Kazakhstan). In: Coleman RG, Wang X (eds) Ultrahigh-pressure metamorphism. Cambridge University Press, Cambridge pp 427–455
Shatsky VS, Jagoutz E, Sobolev NV, Kozmenko OA, Parkhomenko VS, Troesch M (1999) Geochemistry and age of ultrahigh pressure metamorphic rocks from the Kokchetav Massif (Northern Kazakhstan). Contrib Mineral Petrol 137:185–205
Smith DC (1984) Coesite in clinopyroxene in the Caledonides and its implications for geodynamics. Nature 310:641–644
Sobolev NV, Shatsky VS (1990) Diamond inclusions in garnets from metamorphic rocks: a new environment for diamond formation. Nature 343:742–746
Storre B (1972) Dry melting of muscovite + quartz in the range Ps = 7 kb to Ps = 20 kb. Contrib Mineral Petrol 37:87–89
Susaki J, Akaogi M, Akimoto S, Shimura O (1985) Garnet–perovskite transformation in CaGeO3: in-situ X-ray measurements using synchrotron radiation. Geophys Res Lett 12:729–732
Terry MP, Robinson P, Krogh-Ravna EJ (2000a) Kyanite eclogite thermobarometry and evidence for thrusting of UHP over HP metamorphic rocks, Nordoyane, Western Gneiss Region, Norway. Am Mineral 85:1637–1650
Terry MP, Robinson P, Hamilton MA, Jercinovic MJ (2000b) Monazite geochronology of UHP and HP metamorphism, deformation, and exhumation, Nordoyane, Western Gneiss Region, Norway. Am Mineral 85:1651–1664
Verhoogen J (1954) Petrological evidence on temperature distribution in the mantle of the Earth. Trans Am Geophys Union 35(1):85–92
Verhoogen J (1973) Possible temperatures in the oceanic upper mantle and the formation of magma. Geolo Soc Am Bull 84(2):515–521
Vielzeuf D, Clemens JD (1992) The fluid-absent melting of phlogopite + quartz: experiments and models. Am Mineral 77:1206–1222
Vielzeuf D, Montel JM (1994) Partial melting of Al-metagreywackes. Part I Fluid-absent experiments and phase relationships. Contrib Mineral Petrol 117:375–393
Vielzeuf D, Schmidt M (2001) Melting relations in hydrous systems revisited: application to metapelites, metagreywackes and metabasalts. Contrib Mineral Petrol 141:251–267
Vielzeuf D, Cavallini M, Laporte D (1994) Experimental segregation of partial melts from pelites and greywackes. AGU Spring meeting may 23–27. EOS 75, 16, 360
Wallis S, Tsuboi M, Suzuki K, Fanning M, Jiang L, Tanaka T (2005) Role of partial melting in the evolution of the Sulu (easter China) ultrahigh-pressure terrane. Geology 33:129–132
Wang X, Liou JG, Mao HK (1989) Coesite-bearing eclogites from the Dabie Mountains, central China. Geology 17:1085–1088
Wang QC, Ishiwatari A, Zhao Z, Hirajima T, Enami M, Zhai M, Li J, Cong BL (1993) Coesite-bearing granulite retrograded from eclogite in Weihai, eastern China. Eur J Mineral 5:141–152
Wyllie PJ, Wolf MB (1993) Amphibolite dehydration-melting: sorting out the solidus. In: Prichard HM, Alabaster T, Harris NBW, Neary CR (eds) Magmatic processes and plate tectonics. Geol Soc Spec Publ 76:405–416
Xiao Y, Hoefs J, van den Kerkhof AM, Fiebig J, Zheng Y (2000) Fluid history of UHP metamorphism in Dabie Shan, China: a fluid inclusion and oxygen isotope study on the coesite-bearing eclogite from Bixiling. Contrib Mineral Petrol 139:1–16
Xiao Y, Hoefs J, van den Kerkhof AM, Simon K, Fiebig J, Zheng YF (2002) Fluid evolution during HP and UHP metamorphism in Dabie Shan, China: constraints from mineral chemistry, fluid inclusions and stable isotopes. J Petrol 43(8):1505–1527
Xu ST, Okay AI, Ji S (1992) Diamond from the Dabie Shan metamorphic rocks and its implication for the tectonic setting. Science 256:80–82
Yao Y, Ye K, Liu J, Cong B, Wang Q (2000) A transitional eclogite- to high pressure granulite-facies overprint on coesite–eclogite at Taohang in the Sulu ultrahigh-pressure terrane, Eastern China. Lithos 52:109–120
Zen E-An (1986) Aluminum enrichment in silicate melts by fractional crystallization; some mineralogic and petrographic constraints. J Petrol 27:1095–1117
Zhang J, Li B, Utsumi W, Liebermann RC (1996) In-situ X-ray observation of the coesite–stishovite transition: reversed phase boundary and kinetics. Phys Chem Miner 23:1–10
Zhang Z, Xu Z, Xu H (2000) Petrology of ultrahigh-pressure eclogites from the ZK703 drillhole in the Donghai, eastern China. Lithos 52(1–4):35–50

Zhang H, Zhong Z, Gao S, Zhang B, Li H (2001) U–Pb zircon age of the foliated garnet-bearing granites in western Dabie Mountains, Central China. Chin Sci Bull 46(19):1657–1660

Zhong Z, Zhang H, Suo S, You Z (1999) Partial melting processes during exhumation of ultrahigh-pressure metamorphic rocks in Dabieshan, China. J China Univ Geosci 10(3):194–199

Zhong Z, Suo S, You Z, Zhang H, Zhou H (2001) Major constituents of the Dabie collisional orogenic belt and partial melting in the ultrahigh-pressure unit. Int Geol Rev 43:226–236